Bioorganic Chemistry 143 (2024) 107091

Contents lists available at ScienceDirect

Bioorganic Chemistry

journal homepage: www.elsevier.com/locate/bioorg

C_3-Spirooxindoles: Divergent chemical synthesis and bioactivities (2018–2023)

Mohamed H. Helal [a], Medhat E. Owda [b], Amal T. Mogharbel [c], Ali Hamzah Alessa [c], Noha Omer [c], Mahmoud A. Abdelaziz [c], Islam Ibrahim [b,d], Essam M. Eliwa [b,e,*]

[a] Department of Chemistry, Faculty of Arts and Science, Northern Border University, Rafha, 91911, PO 840, Saudi Arabia
[b] Chemistry Department, Faculty of Science (Boys), Al-Azhar University, Nasr City 11884, Cairo, Egypt
[c] Department of Chemistry, Faculty of Science, University of Tabuk, Tabuk 71491, Kingdom of Saudi Arabia
[d] Department of Chemistry and Biochemistry, Florida International University, Miami, FL 33199, USA
[e] Institute of Chemistry of Strasbourg, UMR 7177–LCSOM, CNRS, Strasbourg University, 4 Rue Blaise Pascal, 67000 Strasbourg, France

ARTICLE INFO

Keywords:
Spirooxindole
Chemical synthesis
Reaction mechanism
Bioactivity
Molecular docking

ABSTRACT

This scientific review documents the recent progress of C_3-spirooxindoles chemistry (synthesis and reaction mechanism) and their bioactivities, focusing on the promising results as well as highlighting the biological mechanism via the reported molecular docking findings of the most bioactive derivatives. C_3-Spirooxindoles are attractive bioactive agents and have been found in a variety of natural compounds, including alkaloids. They are widely investigated in the field of medicinal chemistry and play a key role in medication development, such as antivirals, anticancer agents, antimicrobials, etc. Regarding organic synthesis, several traditional and advanced strategies have been reported, particularly those that started with isatin derivatives.

1. Introduction

Because of their widespread distribution in natural products and synthesized compounds with potential bioactivities, spiroheterocycles are regarded as a preferred framework. Among them are C_3-spirooxindoles, which have a flexible biological profile produced by several natural and synthetic analogues derived from the combination of C-3 indolyl scaffolds with numerous heterocycles providing various patterns such as horsfiline, elacomine, isoelacomine, rhynchophylline, spirotryprostatin B, and trigolute D [1,2] (Fig. 1). C_3-Spirooxindoles have wide pharmaceutical implementations as anticancer, anti-inflammatory, antimicrobial, antiviral, antidiabetic, and antimalarial agents [3] (Fig. 2).

Spirooxindole chemical synthesis is a fast-emerging research topic in which large-scale studies are being conducted on techniques for green, sustainable, catalytic, and asymmetric synthesis. As starting materials for spirooxindole synthesis, isatin derivatives coupled with amines, active methylene compounds/α,β-unsaturated molecules are often used. MCRs are one-pot synthetic processes in which more than two reactants mix sequentially to produce highly selective products that retain the bulk of the starting material's atoms. MCRs are a key technique in the development of novel drugs. MCRs are frequently expanded into combinatorial, solid-phase, or flow syntheses for the development of novel lead structures of active drugs. Clearly, MCRs are desirable and usable among the many synthetic techniques [1]. Over the last decade, several review publications have reported on the synthesis techniques and biological features of spirooxindoles [2–7]. Given the biological importance and synthetic hurdles of spirooxindole creation, there is an urgent need to gather recent discoveries in the field. This scientific review summarizes the newly discovered approaches for accessing distinct C_3-spirooxindoles categorized according to their medicinal features and uses throughout the previous six years (2018–2023).

2. Synthesis of C_3-spirooxindoles via spirocyclization of isatin derivatives as traditional protocols

2.1. Chemical synthesis of anticancer C_3-spirooxindoles

Wu *et al.*'s (2018) paper successfully documents the chemical synthesis of a group of C_3-spirooxindoles-linked tetrazolo[1,5-*a*]pyrimidine units **4a–o** (Scheme 1). The classic multicomponent condensation reaction of isatins (**1**), lawsone (hennotannic acid, **2**), and 5-aminotetrazole (**3**) in acetic acid under refluxing conditions yielded the

* Corresponding author at: Chemistry Department, Faculty of Science (Boys), Al-Azhar University, Nasr City 11884, Cairo, Egypt.
E-mail address: essameliwa85@azhar.edu.eg (E.M. Eliwa).

https://doi.org/10.1016/j.bioorg.2023.107091
Received 20 September 2023; Received in revised form 26 December 2023; Accepted 31 December 2023
Available online 4 January 2024

Abbreviations

MCRs	Multicomponent reactions
MW	Microwave
TEMPO	2,2,6,6-Tetramethyl-1-piperidinyloxy
TFE	Trifluoroethanol
DCM	Dichloromethane
DFT	Density functional theory
WHO	World Health Organization
IC_{50}	Half-maximal inhibitory concentration
CC50	50 % Cytotoxic concentration
EC50	Half maximal effective concentration
MIC	Minimum inhibitory concentration
GI50	The growth inhibitory power
K_D	the concentration of antibody
Ki	The inhibitor constant
NCI	The National Cancer Institute, USA
MTT	3-(4,5-Dimethylthiazol-2-yl)-2,5-diphenyltetrazolium bromide
CDK4	Cyclin-dependent kinase 4
EGFR	Epidermal growth factor receptor
GPX4	Glutathione peroxidase 4
MDM2	Mouse double minute 2 homolog
PGE2	Prostaglandin E2
TNF-α	Tumor necrosis factor alpha
COVID-19	Coronavirus infectious disease 2019
SARS-CoV-2	Severe acute respiratory syndrome coronavirus 2
DENV-1/2/3	Dengue virus serotype 1/2/3

Cancer cell lines

HepG2	Human liver cancer cell line
LO2	Human fetal hepatocyte cell line
SKOV-3, A2780	Ovarian cancer cell lines
A549	Lung cancer cell line
MCF-7, MDA-MB-453	Human breast cancer cell lines
LNCaP, DU145	Human prostate cancer cell lines
SJSA-1	Human Osteosarcoma
HCT 116, CT26, Caco-2	Colon cancer cell lines
U87MG, U251, T98G	Glioblastoma cell lines
PC3	Prostate cancer cell
SKNSH	Human neuroblastoma cell line
Hela	Cervical cancer cell line
EC109	Esophageal squamous cell carcinoma
MGC803	Gastric mucinous adenocarcinoma

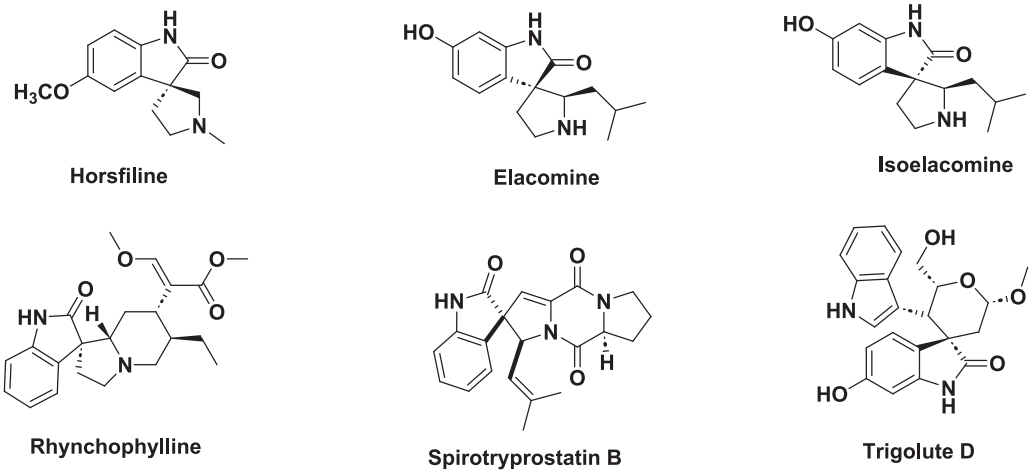

Fig. 1. Natural C_3-spirooxindoles.

corresponding C_3-spirooxindoles **4a–o** in weak to moderate isolated yields (31–69 %) for 5–8 h. The proposed mechanism for the creation of **4a–o** is displayed in Fig. 3. Isatins (**1**) undergo Knoevenagel condensation with 2-hydroxy-1,4-naphthoquinone (**2**) to form the corresponding olefin, which condensed with 5-aminotetrazole (**3**) to form the corresponding ketimine. Subsequent intramolecular cyclization via aza-Michael addition reaction (1,4-conjugate addition) of ketimine afforded the desired C_3-spirooxindole products (**4a–o**). In comparison with tanshinone IIA reference drug [IC_{50} = 23.85 (HepG2), 65.29 (LO2) μM], compounds (**4a–o**) possess a potent cytotoxic property towards HepG2 with mean IC_{50} values ranging from 2.86 to 36.34 μM, but the normal LO2 cell line was less susceptible (IC_{50} = 36.37–248.39 μM). R substituents (5-F, 5-Me, 7-Cl, and 7-CF3) showed the best anti-proliferative potency. The authors did not examine the stereochemistry of **4a–o** [8].

In the same synthesis manner, Ghosh *et al.*'s (2020) research article provides the chemical synthesis of a set of C_3-spirooxindoles-linked *N*-methyl pyrrolidine/pyrrolizidine units **7a–e**/**8a–e** (Scheme 2). These hybrids were installed via a one-pot protocol featuring MCR and stereoselectivity in good to excellent yields (76–93 %) employing ethanol as a solvent at the reflux temperature for 5 h. The reaction seems to proceed by the [3 + 2] cycloaddition mechanism of dipole azomethine ylides [*in situ* formed from **1** with sarcosine (*N*-methylglycine, **6a**)/L-proline (**6b**)] and dipolarophiles **5**. The mechanistic study for the formation of **8a–e** is shown in Fig. 4. As a widely common pathway for the creation of C_3-spirooxindoles, *especially in this article review*, S-shaped dipole azomethine ylide was generated *in situ* while heating **1** and **6b**. As a significant route to the regio- and stereoselective organic synthesis of five-membered heterocycles, *endo* 1,3-dipolar cycloaddition between 1,3-dipole and α,β-unsaturated ketone dipolarophile reagent **5** yielded the corresponding C_3-spirooxindoles **8a–e**. The newly developed spirooxindoles (**7a–e**/**8a–e**) were evaluated for antiproliferative potency towards NCI-60 tumor cell lines and DNA G-quadruplex binding affinity. Biologically speaking, at a concentration of 10 μM, molecule **8b** (R = 4-Br, R_1 = 4-Cl) demonstrated specific cytotoxicity towards some carcinoma cell lines (colon, leukemia, prostate, and renal). G4 interaction tests revealed that these C_3-spirooxindoles have little activity as DNA G-quadruplex ligands [9].

By the same token, Mayakrishnan *et al.*'s (2022) study effectively

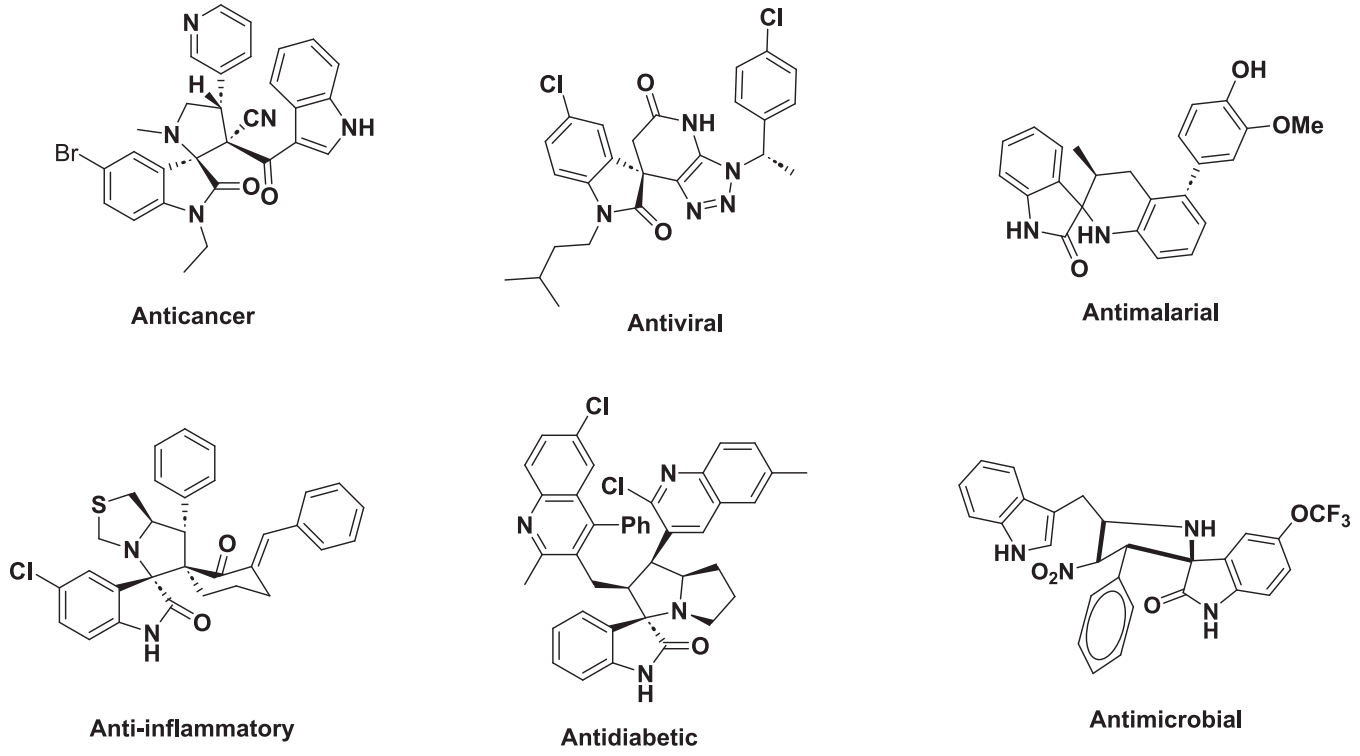

Fig. 2. Bioactive molecules containing a C_3-spirooxindole unit.

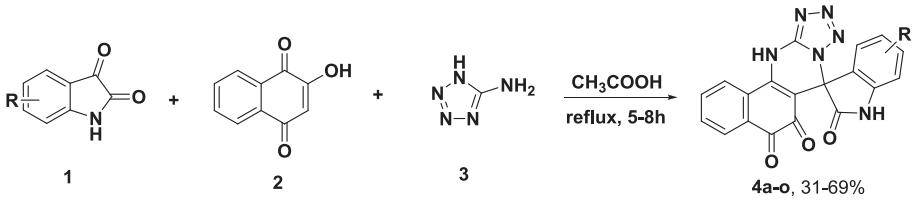

R = H, 5-Br, 5-Cl, 6-Br, 1-CH_3-7-F, 7-Cl, 5-F, 7-Br, 1-C_6H_5, 5-CH_3, 6-Cl, 6-OCH_3, 5-OCF_3, 7-CF_3

Scheme 1. Chemical construction of C_3-spirooxindoles-linked tetrazolo[1,5-*a*]pyrimidine units **4a–o**.

details the chemical synthesis of a group of C_3-spirooxindoles-bearing indole and pyridine moieties (**10a–x**) in good to excellent yields (75–96 %) under reflux conditions in EtOH for 2.5–3.0 h. Also, these molecules were constructed via a one-pot stereoselective protocol based on the [3 + 2] cycloaddition process between azomethine intermediates (*in situ* produced from **1** with secondary amines **6a–c**) and dipolarophile reagents **9a** and **9b** (Schemes 3). Using the MTT bioassay, these newly created compounds (**10a-x**) were tested for anticancer efficacy against three carcinoma cell lines (HepG2, SKOV-3, and A549). In comparison with cisplatin, which was not active towards HepG2 cells, **10u** and **10w** had higher cytotoxic actions towards them at concentrations less than 10 μg/mL. To get insights of biological mechanism, molecular docking simulation by Auto Dock Tools (ADT) version 1.5.6 and Auto Dock Version 4.2.5.1 was conducted between C_3-spirooxindoles (**10a–10x**) with BCL-2 (PDB ID: 4IEH) and ALK receptors (PDB ID: 2XP2). Compound **10w** showed the best binding mode with BCL-2 (-8.41 kcal/mol) via interaction with seven amino acid residues. Among them two H-bonds are formed between the C═O of Val92 and the N—H of indole moiety and the second one is generated between the C═O of Asp70 and the N—H of the pyrrole ring of isatin. Regarding ALK receptors, compound **10o** exhibited the best binding affinity (-7.14 kcal/mol) through a variety of intermolecular interactions. Three of them are conventional H-bonds, which installed between the indole ring and Leu1122, pyridine ring and Ala1126, and the last one is existed between the isatin C═O and Lys1150 [10].

MDM2 and MDM4 are important negative regulators of p53, which is classified as a tumor suppressor gene. In response to stress, the tumor suppressor p53 can transcriptionally activate downstream genes, which subsequently control several cell processes, including the cell cycle, DNA repair, metabolism, angiogenesis, apoptosis, and other biological responses. The p53 signaling pathway is shown in Fig. 5. The p53 tumor suppressor function is inactivated in tumors overexpressing MDM2 and MDM4 proteins. Hence, these two proteins are significant targets for cancer therapy, aiming to reactivate of the p53 function [11–13]. Some C_3-spirooxindoles have been found to be MDM2-p53 inhibitors and are now being studied in humans (Fig. 6) [14].

The MW-assisted construction of C_3-spirooxindoles **12** as a racemic mixture is effectively shown in the study by Gollner *et al.* (2019). Next, the obtained mixture **12** was subjected to a reductive amination with cyclopropanecarboxaldehyde in the presence of $NaBH(OAc)_3$ to furnish **13** that was followed by the Buchwald C—N coupling reaction (Cs_2CO_3, Xantphos, $Pd(TFA)_2$, MW) with methyl *p*-bromobenzoate, yielding C_3-spirooxindoles-linked pyrrolidine fused pyrrolidinone **14** in good yield (86 %) (Scheme 4). The anticancer efficiency of **14** against MDM2-p53 was highly robust (IC_{50} = 4 nM). As shown in Fig. 7, the authors succeeded in obtaining the X-ray crystal structure of compound **13** interacted with the active site of MDM2, where the most important H-bond between the amino acid residue His96 and the lactam C═O was formed

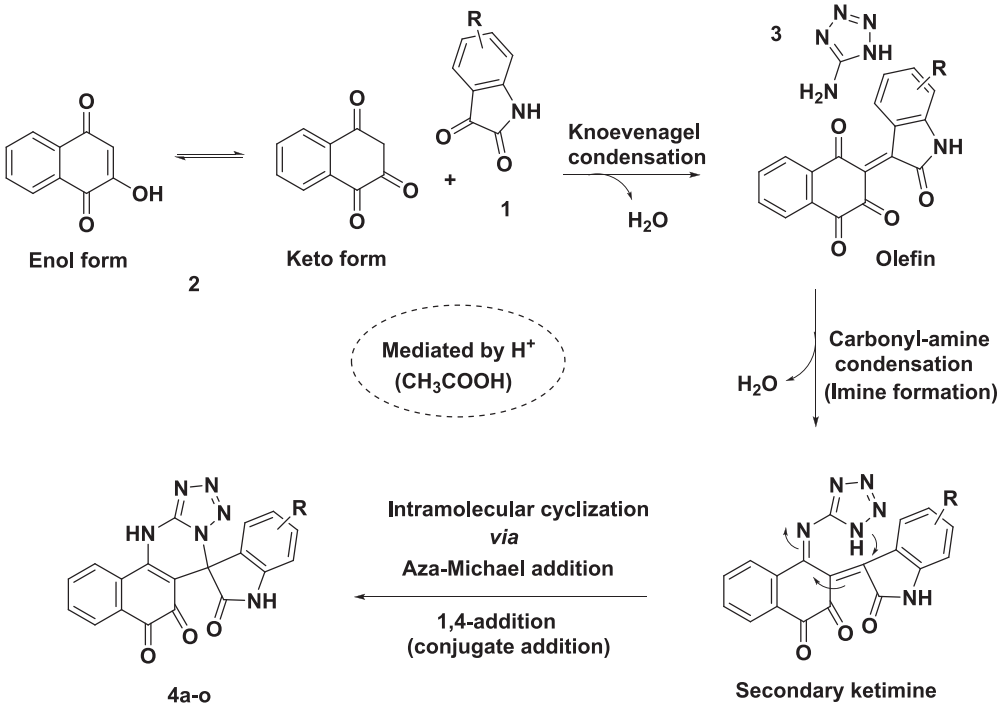

Fig. 3. The proposed mechanism for the construction of **4a–o**.

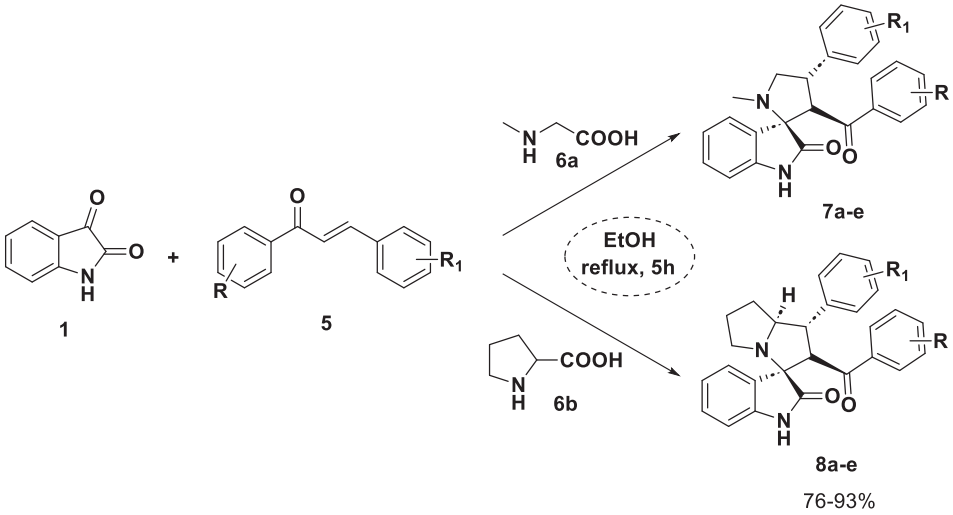

Scheme 2. Chemical construction of C_3-spirooxindoles-linked *N*-methyl pyrrolidine/pyrrolizidine units **7a–e**/**8a–e**.

[15].

Most recently, Islam et al.'s (2023) study describes the pharmacophoric hybridization design and chemical construction of a new library of C_3-spirooxindoles-linked pyrazole **16a–o** (isolated with yields up to 76–98 %) targeting the MDM2-p53. As aforementioned, the target molecules were constructed via stereoselective, one-pot, MCR based on [3 + 2] cycloaddition between azomethine ylides (*in situ* produced from **1** with **6c**) and dipolarophile chalcones-based pyrazole core **15a–o** (Schemes 5). In comparison with doxorubicin [7.7 ± 3.9 (A2780), 61.3 ± 15.2 (A549), 178 ± 26 (MDA-MB-453), and 127 ± 18 nM (HepG2)], MTT bioassay results showed that compound **16 h** was the best towards A2780 and HepG2, with IC_{50} mean values of 10.3 and 18.6 μM, respectively. Meanwhile, **16 m** was the robust one against A549 with an IC_{50} value of 17.7 μM. MDM2 was downregulated in A549 cells by **16 k** and **16 m**, according to Western blot analysis. In combination with doxorubicin, **16 h** and **16j** were reduced its IC_{50} by 25 % [16].

Regarding the biological mechanism, the docking study of **16 k** and **16 m** against MDM2 (PDB ID: 5LAW) was done by the "QuickPrep" of the Molecular Operating Environment (MOE) Version 2016.0802. Compound **16 k** was fitted within the active site of MDM2 with binding energy value of −5.49 kcal/mol via several interactions. Importantly of them is the H-bond that installed between the linker C=O and His96, which interacted with indolinone ring through π-π hydrophobic interaction. On the hand, compound **16 m** was interlocked with the active domain of MDM2 by binding score value of −6.01 kcal/mol that slightly better than **16 k**, but without H-bond interactions. His96 forms π-π hydrophobic interaction with *N*-phenylpyrazole moiety instead of indolinone ring [16].

In 2022, Espadinha and his co-workers reported the structural optimization and the chemical construction of a library of C_3-spirooxindole-linked pyrazoline (**20**). Installation of these hybrids started with formation of ethyl ester **19** via the cycloaddition reaction of **17** and

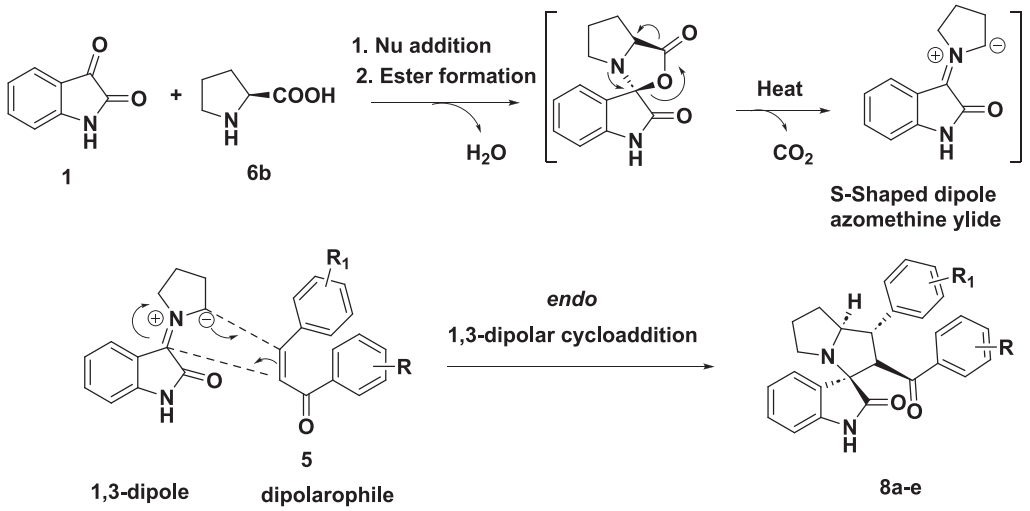

Fig. 4. The proposed mechanism for the construction of **8a–e**.

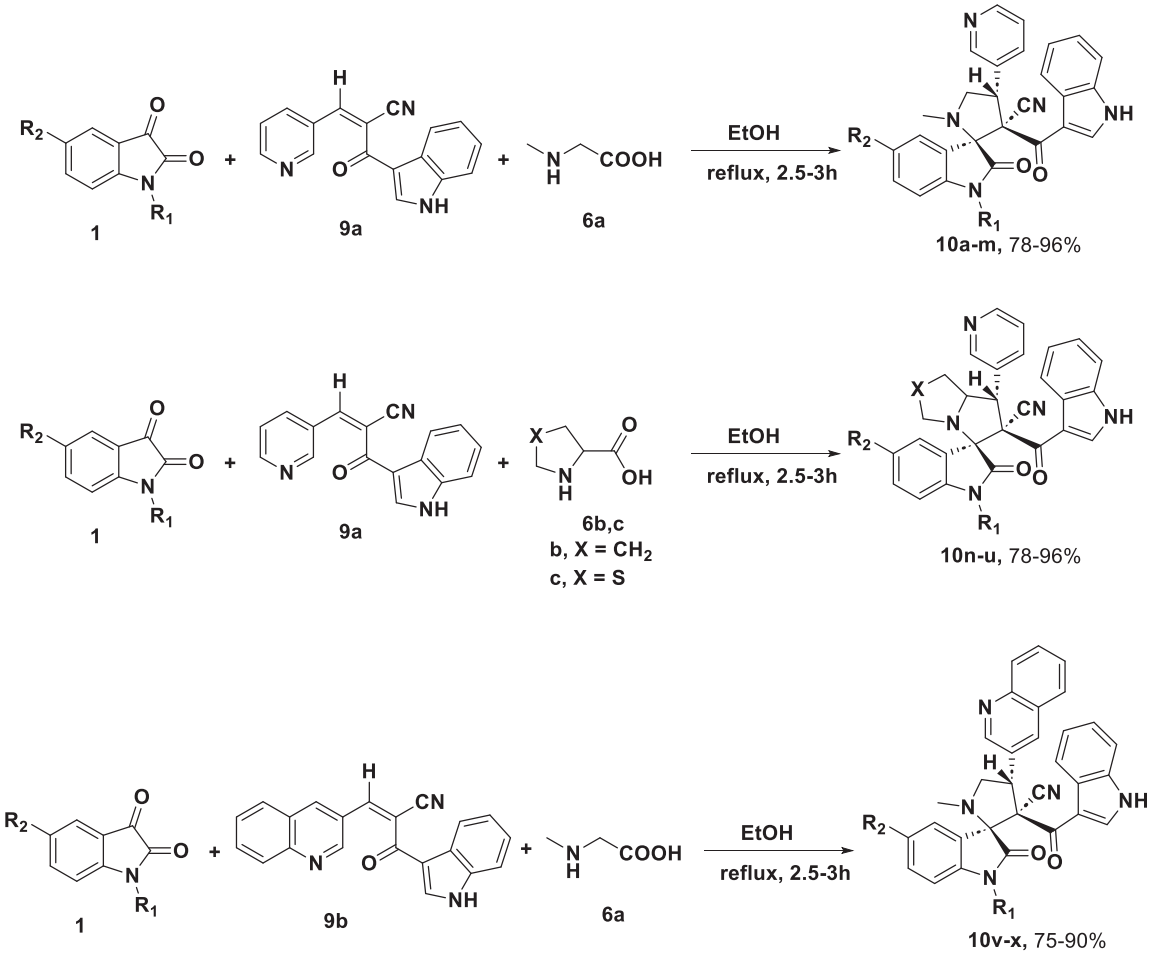

Scheme 3. Chemical construction of C_3-spirooxindoles-bearing indole and pyridine moieties **10a–x**.

hydrazonyl chlorides **18**. The sequential alkaline hydrolysis-amination process of **19** yielded the hit pyrazoline amides **20** (Scheme 6). Many of the generated molecules have shown potential antiproliferation activities towards MCF-7, LNCaP, and SJSA-1 tumor cells by dual blocking MDM2-P53 and MDM4-p53 interactions. Immunoenzymatic biochemical assay showed that **20a** (R = 6-Cl, R′ = 3-Cl-2-F-Ph, R″ = $CO_2CH_2CH_3$, R‴ = cyclohexyl) was the most potent dual inhibitor towards MDM2-P53 and MDM4-p53 in the low nanomolar range, with IC_{50} values of 18.5 ± 2.1 and 14.8 ± 5.2 nM, respectively. *In silico* rational design studies interpret the prior activity, where Fig. 8 shows the main interaction types between **20** and MDM2/4-P53 [17].

The work of Lotfy *et al.* (2021) indicates the rational design and the

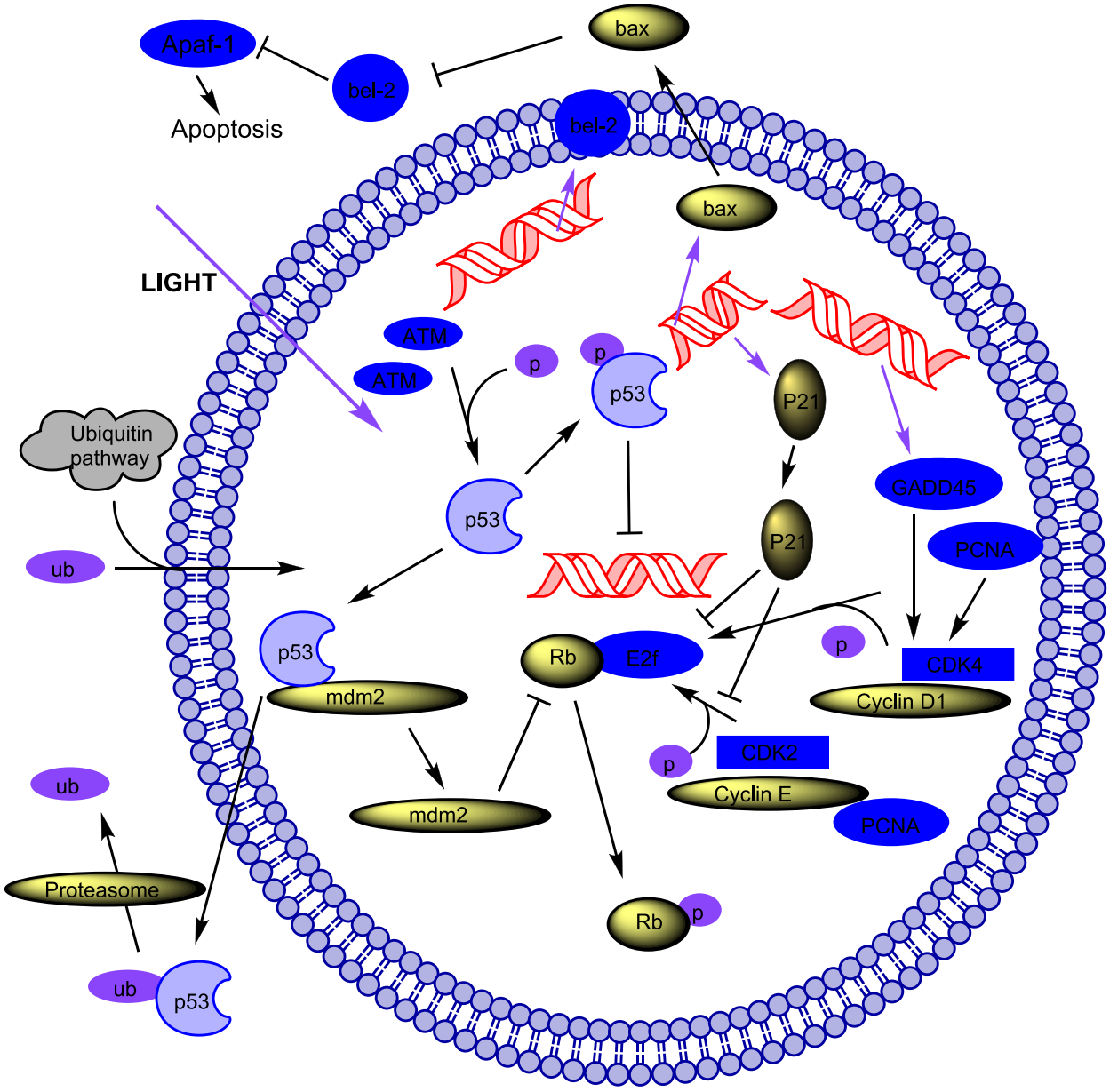

Fig. 5. The p53 signaling pathway. Reproduced from the ChemOffice-v2022.

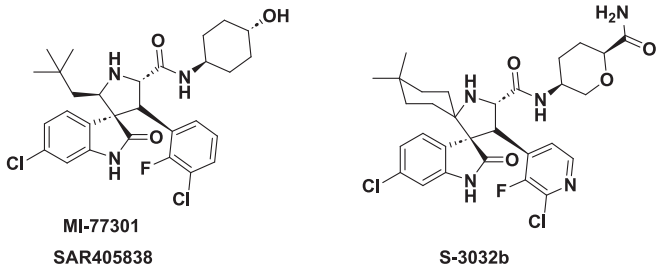

Fig. 6. MDM2-p53 inhibitors-based C_3-spirooxindole unit.

traditional construction of stereospecific C_3-spirooxindoles-bearing hydropyrrolizine unit **22** (87–95 %) that were synthesized by a one-pot 1,3-dipolar cycloaddition of azomethine intermediates and pyrrole derivatives **21** (Scheme 7). Stereoselectivity in this protocol was validated by quantum chemical computations through DFT. The *in vitro* NCI-60 one-dose screening methodology was used to evaluate the anti-proliferation activity of **22** towards subpanel human carcinoma cell lines (leukemia, lung, colon, CNS, melanoma, ovary, kidney, prostate, and breast cancers) at 10 μM concentration. NCI-60 anticancer screening activities were expressed as percentage growth inhibition (GI %) [18]. Many of the obtained molecules demonstrated good MDM2 inhibitory activities. Using MTT biochemical assay, the potent compounds from the NCI-60 protocol were tested against MDA-MB 231, HepG2, and Caco-2 cancer cells. In comparison with 5-fluorouracil, the installed compounds **22a** and **22b** (Scheme 7) were more active towards MDM2 binding ability in the low μM range, with K_D values of 1.32 and 1.72 μM, respectively [18]. The docking study of compounds **22a** and **22b** was done as earlier mentioned above for compounds **16 k** and **16 m** [16] (Scheme 5). The best binding modes of **22a** and **22b** show the important role of indolinone rings that form the key intermolecular H-bonds with Leu54 for **22a** and His96 with Lys94 for **22b** [18].

In a similar synthetic vein, C_3-spirooxindoles possessing furan moiety **23** (Scheme 8) were successfully constructed (isolated yield up to 94 %) through a one-pot protocol that published by Altowyan research

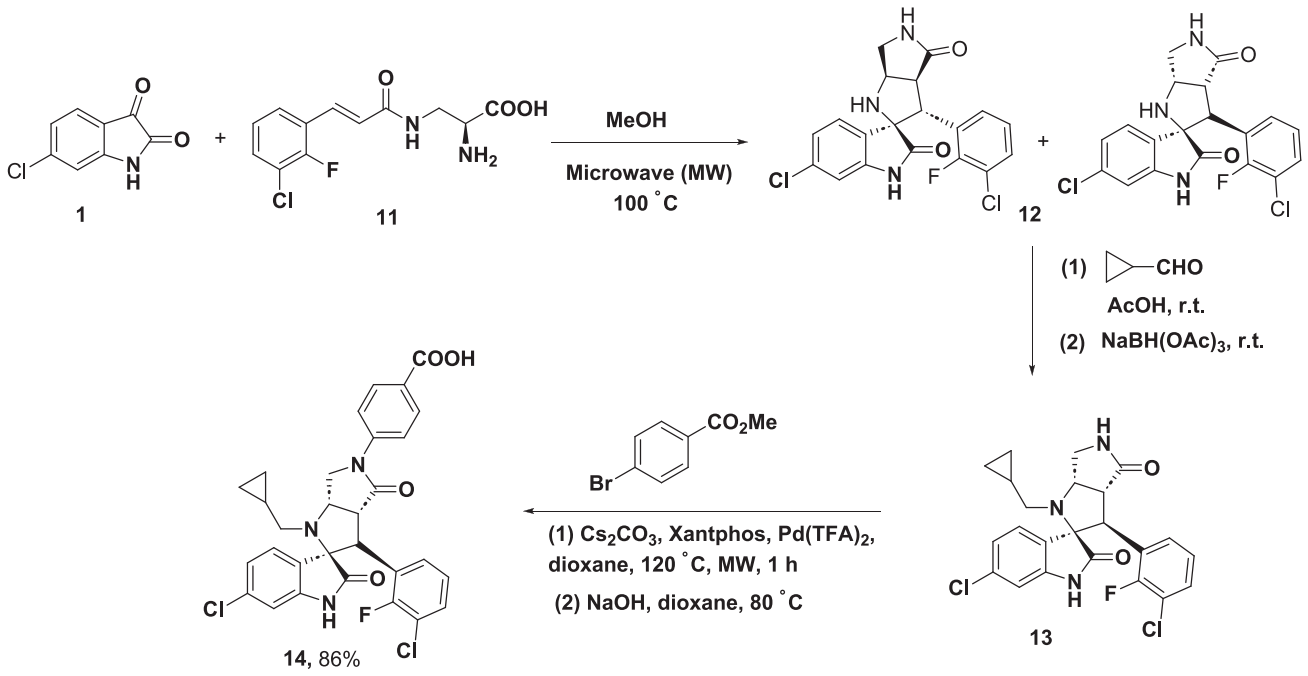

Scheme 4. Chemical construction of C_3-spirooxindoles-linked pyrrolidine fused pyrrolidinone **14**.

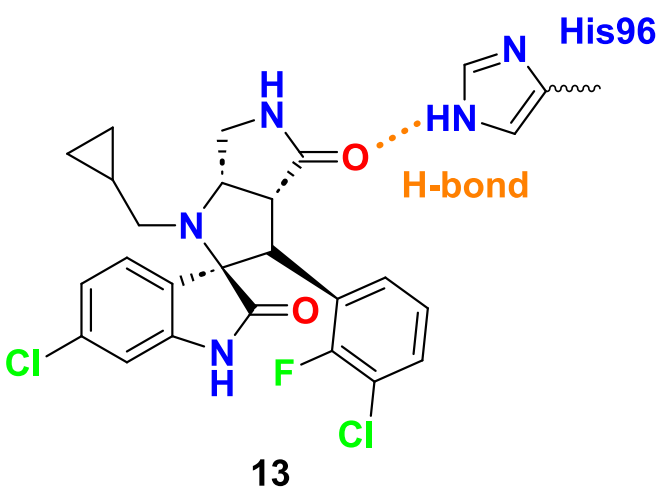

Fig. 7. The main interaction of **13** with MDM2-p53.

group in 2022. In comparison to the reference medication staurosporine [IC_{50} = 17.8 ± 0.50 (MCF-7) and 10.3 ± 0.23 (HepG2) μM/mL], two of the prepared compounds (**23a** and **23b**) demonstrated strong anticancer activity against HepG2 and MCF-7 carcinoma cell lines, with mean IC_{50} values ranging from 4.3 to 11.8 μM/mL [19].

An article from Liu's lab represents the rational design and the construction of CF_3-containing C_3-spirooxindoles-incorporated nitroisoxazole **26** in good to excellent yields (72–93 %) as GPX4-MDM2 dual inhibitors. The construction process was conducted via the stereoselective cycloaddition of 5-styrylisoxazole **25** and imines **24** (Scheme 9). Two of the obtained compounds (**26a** and **26b**) displayed remarkable antitumor activities towards MCF-7 with the inhibition ability of MDM2-p53. In comparison with nutlin-3 [IC_{50} = 15.72 μM (MCF-7) and *Ki* = 0.28 ± 0.0 μM (MDM2)], compound **26a** showed inhibitory effect against MDM2 with *Ki* = 0.24 ± 0.06 μM and cytotoxicity towards MCF-7 with IC_{50} value of 13.5 μM, whilst **26b** exhibited these results: *Ki* = 0.26 ± 0.05 and IC_{50} = 13.7 μM (Scheme 9). The docking study of **26a** towards MDM2 (PDB ID: 4LWU) was operated by CDOCKER module of Discovery Studio 3.5 (Accelrys, USA). The best binding mode shows that the oxindole-N1 forms a stable H-bond with Leu54, while the nitroisoxazole and phenyl groups are stabilized via π-π stacking interactions with His96 [20].

Kukushkin and his co-authors (2021) reported the chemical creation of C_3-spirooxindoles-bearing imidazolone unit **28** in weak to high yields (10–75 %) via a one-pot stereospecific [3 + 2] cycloaddition of 5-indolidene-2-chalcogen-imidazolones **27** and *in situ* generated azomethine intermediate (Scheme 10). Using MTT biochemical cytotoxicity assay and in comparison with Nutlin-3 [IC_{50} = 3.3 ± 0.13 (HCT116 $p53^{+/+}$) and 35.12 ± 2.65 μM (HCT116 $p53^{-/-}$)], among the **28** derivatives, one of its substituted groups, Cl (R), 4-MeOPh (R'), and S (X) showed noticeable cell growth inhibition activities towards HCT116 $p53^{+/+}$ and HCT116 $p53^{-/-}$ with CC_{50} values of 1.95 and 2.35 μM, respectively [21].

In 2020, Wang and his group published the rational design and the asymmetrical creation of C_3-spirooxindoles-linked naphthalenes **32** via the Michael-aldol domino reaction of 3-ylideneisatins **29** and a benzaldehyde derivative **30**. The reaction was mediated by thiourea organocatalyst as a bifunctional hydrogen-bonding source to produce silyl ether analog **31** followed by acid work-up to afford the desired **32** (Scheme 11). The installed compounds successfully suppressed CDK4 and MDM2 in glioblastoma cells. Among the **32** derivatives, one of its substituted groups, 5-Br (R) and CO_2Et (R'), was the most robust and potent towards U87MG, U251, and T98G, with IC_{50} values of 4.9, 8.6, and 9.5 μM, respectively [22].

A library of C_3-spirooxindoles-linked pyrazolopyridine **35** was synthesized via a one-pot three-component cycloaddition reaction of *in situ* formed azomethine intermediates (**1** with 5-aminopyrazole **34**) and aroylacetonitriles **33** under acidic conditions exposed to acetic acid (Scheme 12). In comparison with adriamycin [IC_{50} = 0.12 (HepG2) and 0.62 μM (PC-3)], many of the prepared compounds showed optimistic cell growth inhibition activities. Among the **35** analogs, one of its substituted groups, H (R) and Ph (R'), was the most potent and effective towards HepG2 and PC3, with IC_{50} values of 6.9 and 11.8 μM, respectively. Also, the prior compound displayed high attraction towards p53 and caspase-3/9, confirming their ability to enhance apoptosis. The authors did not examine the stereochemistry of **35** [23,24].

Fayed and his co-authors reported the construction of C_3-

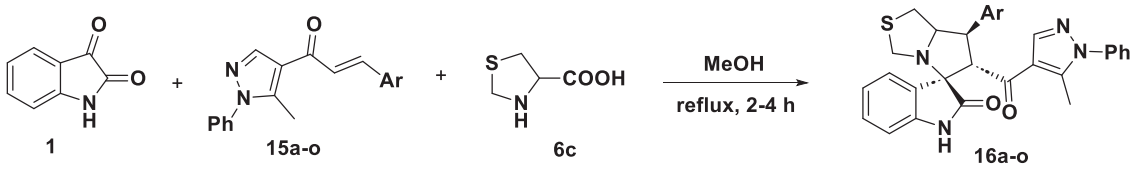

Cpd. No.	Ar	Cpd. No.	Ar	Cpd. No.	Ar
16a	Ph	**16g**	Styryl	**16m**	3-BrPh
16b	2-Furan	**16h**	2,4-diClPh	**16n**	4-NO_2Ph
16c	3-CH_3Ph	**16i**	4-FPh	**16o**	3-NO_2Ph
16d	2-Ferrocene	**16j**	3-FPh	**16p**	4-CH_3Ph
16e	4-CH_3OPh	**16k**	4-CF_3Ph		
16f	4-ClPh	**16l**	2-Py		

Scheme 5. Chemical construction of C_3-spirooxindole-pyrazole hybrids **16a–o**.

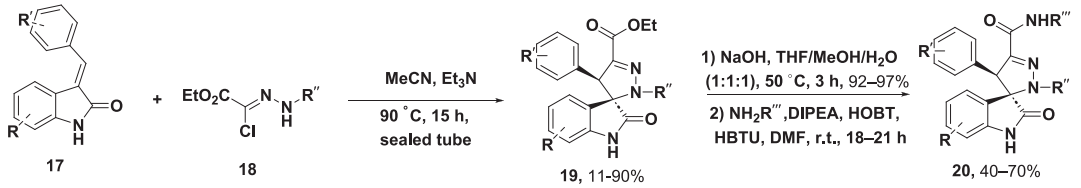

Scheme 6. Chemical construction of C_3-spirooxindole-linked pyrazoline **20**.

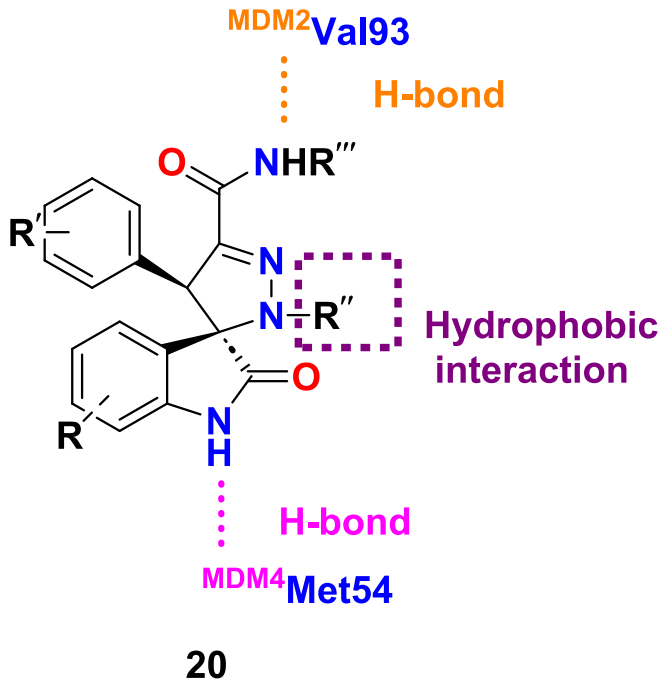

Fig. 8. Main interactions of **20** with MDM2-P53 and MDM4-p53 as indicated from the rational design studies.

spirooxindole-linked chromene heterocycle **37** via Et_2NH-catalyzed the condensation process of **1** and 2'-hydroxyacetophenone. In a similar fashion, compound **36** was installed by using 4'-aminoacetophenone as a ketone. AcOH-catalyzed Schiff base formation between **36** and salicylaldehyde furnishes **38** that was treated with hydrazines in acidic medium to afford the corresponding C_3-spirooxindoles-linked pyrazole heterocycle **39** (Scheme 13). Agents **37** and **39b** displayed optimistic cell growth inhibition activities towards MCF-7, HepG2, and HCT116 with mean IC_{50} values ranging from 0.68 to 1.30 μM, while the reference drug imatinib showed cytotoxic activities with IC_{50} values ranging from 4.70 to 6 μM. Also, **39b** exhibited encouraging EGFR inhibitory potency. The docking study of **39b** against EGFR (PDB ID 1 M17) was done to get an insight into the molecular interaction between them. The docking simulation was performed by MOE v10.2008. The best docking mode of **39b** (-18.76 kcal/mol) manifested three H-bonds between **39b** and EGFR. One among them was between the isatin C=O and Cys773 (2.99 Å) whereas the second one was installed between the salicylaldehyde OH and Lys692 (2.63 Å). The last one was seen between isatin NH and Asp776 (2.46 Å). Also, the phenyl group of salicylaldehyde unit was stabilized via arene-cation interaction with Lys704. The authors did not examine the stereochemistry of **37** and **39** [25].

Kumar *et al.* (2019) reported the first use of ionic liquid [bmim]Br to mediate a one-pot [3 + 2] cycloaddition reaction of azomethine intermediate (*in situ* formed from **1** with tyrosine **6f**) and dipolarophile *β*-nitrostyrenes **40** to yield the C_3-spirooxindoles-linked nitro pyrrolidine unit **41** in good to excellent yields (Scheme 14). A plausible mechanism for the installation of C_3-spirooxindoles-pyrrolidine hybrids **41** is demonstrated in Fig. 9. As a hydrogen donor, ionic liquid [bmim]Br activated the isatin derivatives **1** via hydrogen bonding to form the corresponding imine compound by condensation with **6f**. After subsequent cyclization and decarboxylation steps, the intermediate azomethine ylide was obtained. Hence, 1,3-dipolar cycloaddition between the reactive ylide and the activated nitrostyrenes **40** afforded the desired products **41**. In comparison with camptothecin [IC_{50} = 32.11 ± 2.50 (A549, 48 h) and 22 ± 1.50 μM (Jurkat, 48 h)], MTT bioassay results

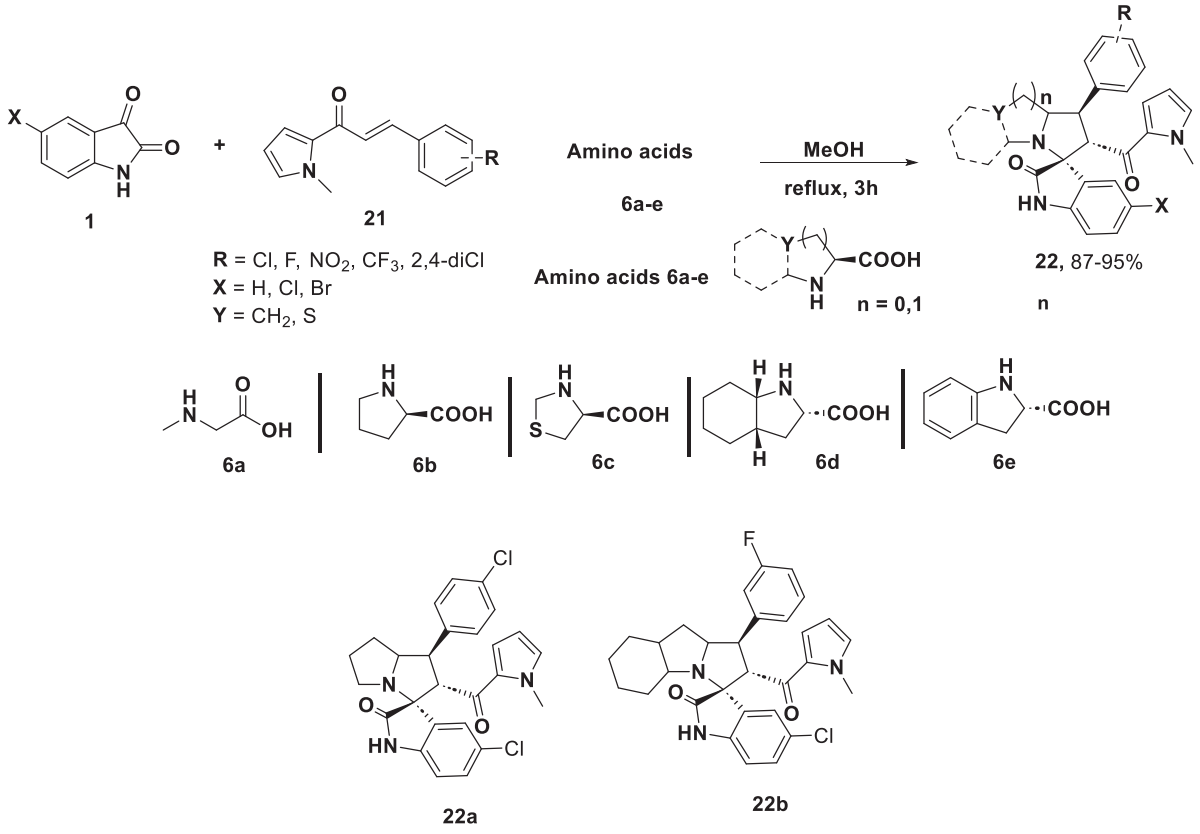

Scheme 7. Chemical construction of C_3-spirooxindoles-bearing hydropyrrolizine unit **22**.

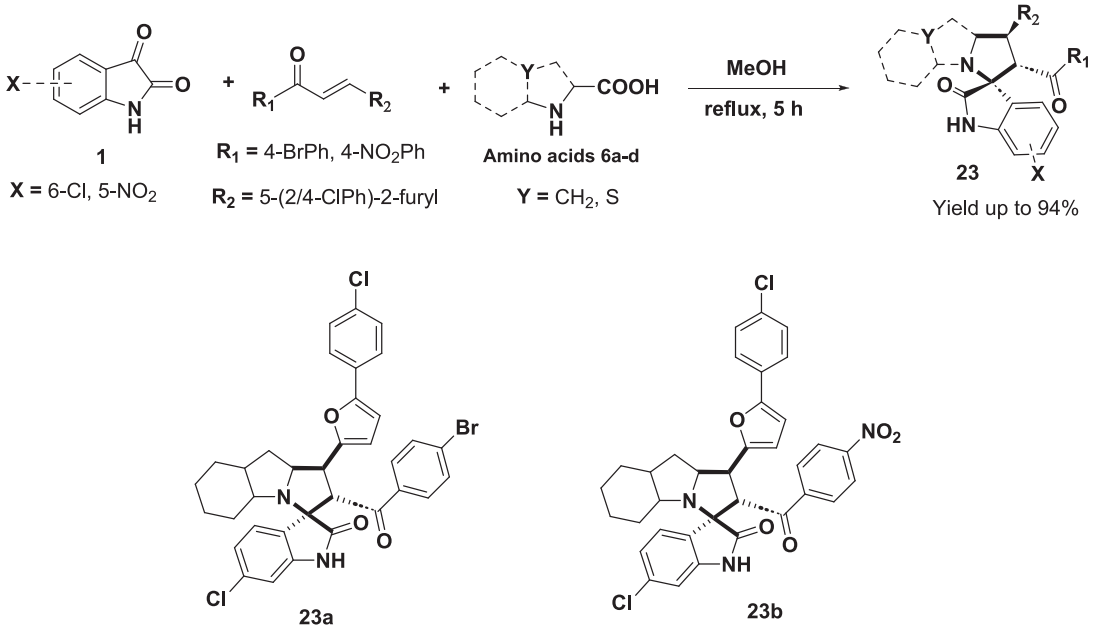

Scheme 8. Chemical construction of C_3-spirooxindoles possessing furan moiety **23**.

showed that one of the **41** analogs that its substituted groups are, 4-OMe (R) and OCF_3 (R'), was the most potent one towards A549 and acute *T*-cell lymphoma (Jurkat cells), with IC_{50} values of 29.60 ± 2.50 and 42.92 ± 4.50 μM (48 h), respectively. The authors did not examine the stereochemistry of **41** [26].

The dipolar [3 + 2] cycloaddition process of azomethine intermediate (*in situ* generated from **1** with 2-piperazinoethylamine **42**) and equimolar amounts of chalcones **5** in stirring EtOH yielded the desired spirooxindoles-linked pyrrolidinone moiety **43** in moderate to good yields (Scheme 15). Among the **43** products in which R = Me, the robust active one towards the KB cell line had a mean IC_{50} value of 6.5 μM [27]. The best molecular docking mode of **43** (R = Me) towards

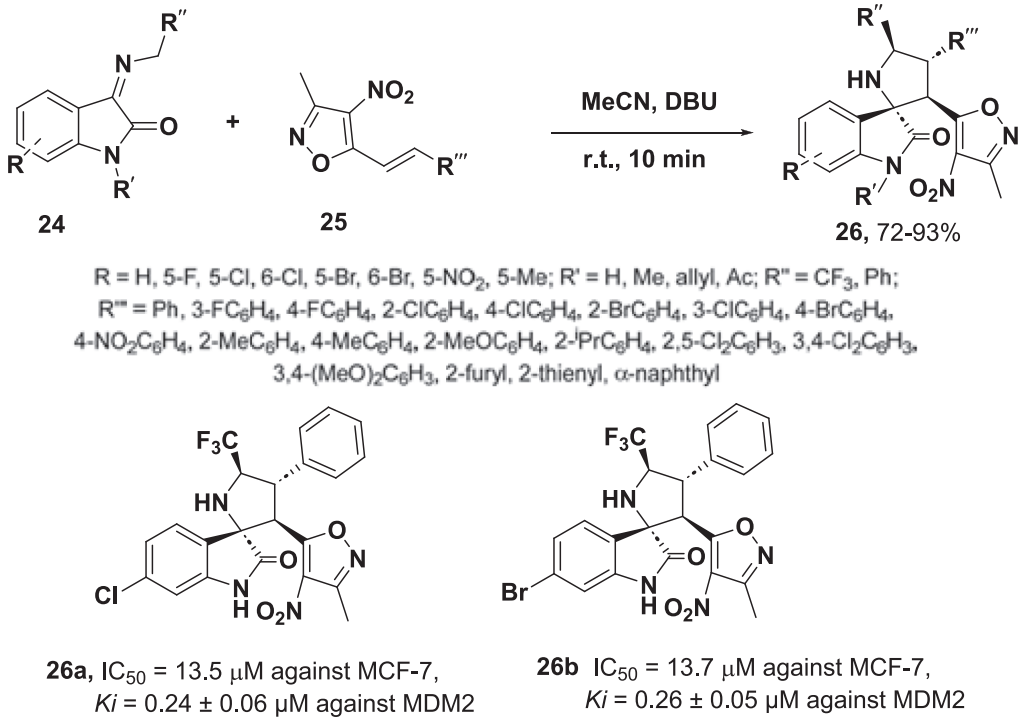

Scheme 9. Chemical construction of C_3-spirooxindoles-incorporated nitroisoxazole core **26**.

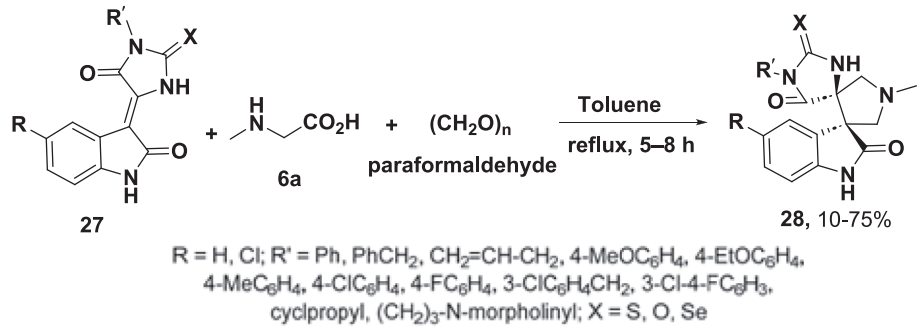

Scheme 10. Chemical construction of C_3-spirooxindoles-bearing imidazolone unit **28**.

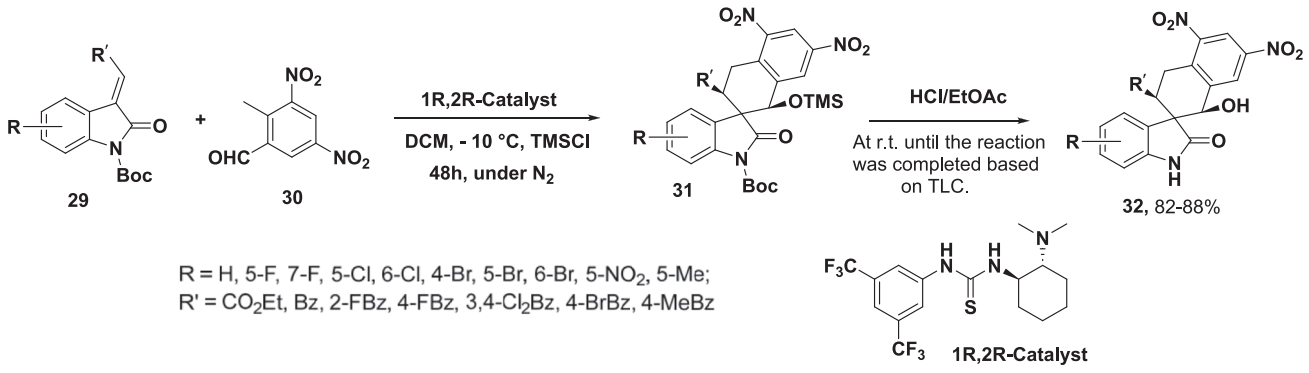

Scheme 11. Chemical construction of C_3-spirooxindoles-linked naphthalenes **32**.

MDM2 (PDB ID: 1RV1) exhibited binding energy value of −12.78 kcal/mol lower than the doxorubicin that was −8.53 kcal/mol. The docking task was achieved by Argus lab and the perception is utilizing discovery studio 4.5. The docked ligand was interlocked into the active site of 1RV1 via several hydrophobic interactions with amino acid residues, including Phe55, Val211, Tyr226, and Phe225. Also, there are *Van der Waals* interactions with Thr233, Lys51, Glu52, Tyr56, Lys221, and Gln59 [27].

In 2019, Islam and his co-workers reported the construction of C_3-spirooxoindoles-linked thiazolopyrrolidine unit **45** in good yields

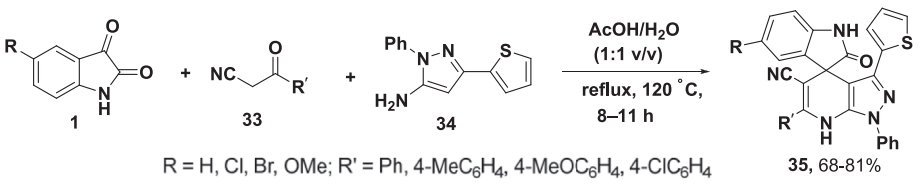

Scheme 12. Chemical construction of C_3-spirooxindoles-linked pyrazolopyridine **35**.

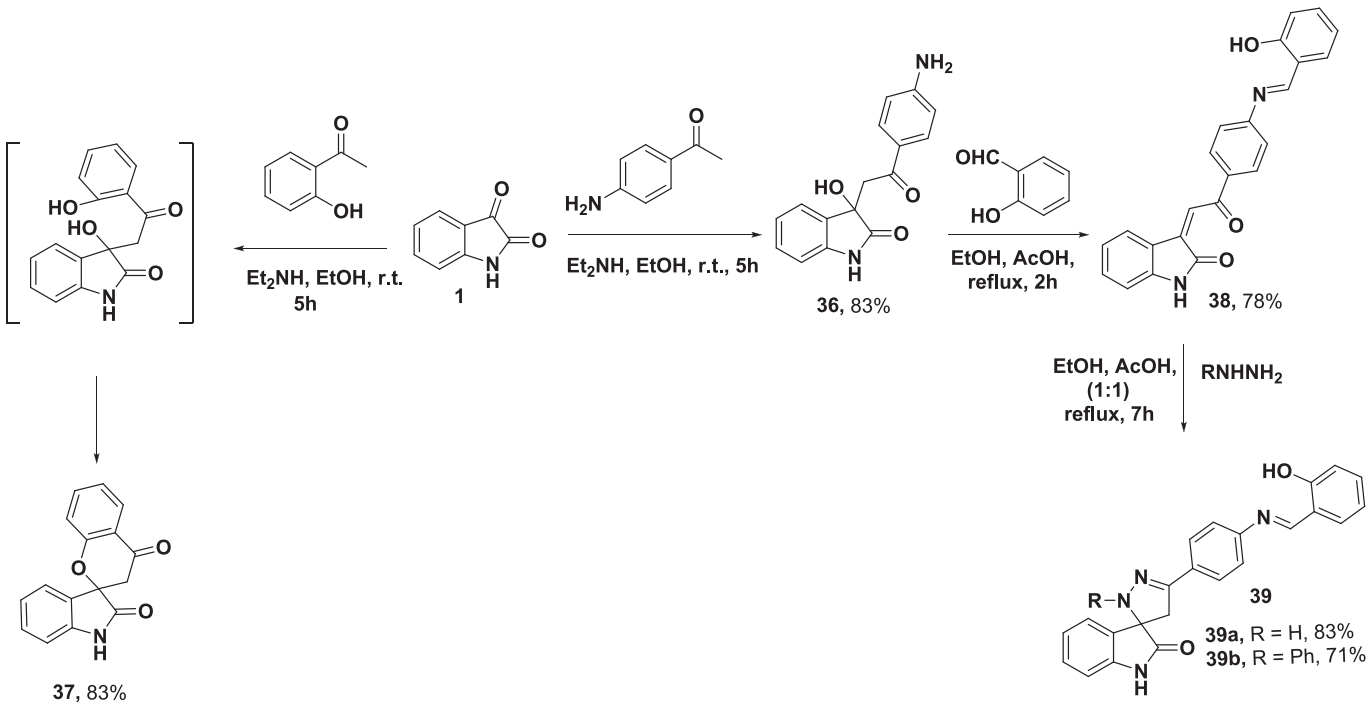

Scheme 13. Chemical construction of C_3-spirooxindole-linked chromene heterocycle **37** and C_3-spirooxindoles-linked pyrazole heterocycle **39**.

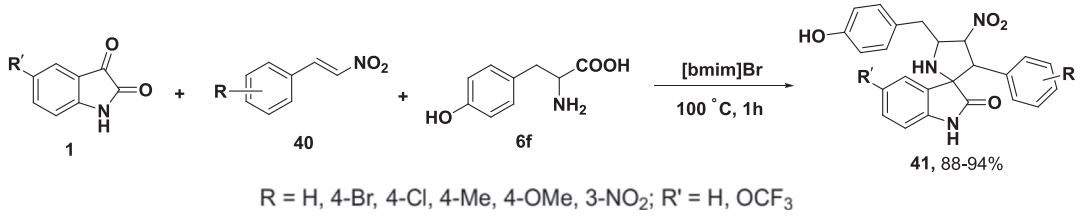

Scheme 14. Chemical construction of C_3-spirooxindoles-linked nitro pyrrolidine unit **41**.

(71–89 %) via a one-pot 1,3-dipolar cycloaddition reaction between azomethine intermediates (*in situ* produced from **1** with **6c**) and dipolarophile chalcones **44** (Schemes 16). In comparison with cisplatin [IC_{50} = 12.6 (HCT116) and 5.5 μM (HepG2)], among the **45** analogs in which R = 4-$CF_3C_6H_4$, the most potent one towards HCT116 and HepG2 carcinoma cell lines had mean IC_{50} values of 7.0 and 5.5 μM, respectively. The best interaction mode between **45** (R = 4-$CF_3C_6H_4$) and MDM2 (PDB code: 5law) was illustrated via the docking study that was operated by Open Eye® software. Most importantly, the simulation mode showed an important H-bond between indole NH (H donor) and Leu54 (H acceptor) [28].

The C_3-spirooxindole-pyrrolocarbazole hybrids **48** were produced in good to excellent yields (73–93 %) by a one-pot [3 + 2] cycloaddition reaction between azomethine intermediates (*in situ* formed from **1** with benzylamine **47**) and dipolarophile 2-ylidene-1*H*-carbazole-1-ones **46** (Schemes 17). Cell growth inhibition abilities were observed for the installed compounds. In comparison with cisplatin [IC_{50} = 9 (MCF-7) and 10 μM (A549)], among the **48** agents in which R'= Me, Cl, and H, were the most potent towards MCF-7 and A549 carcinoma cell lines with IC_{50} values vary from 13 to 16 μM [29].

As reported by the Kasaboina research group in 2019, a library of C_3-spirooxindole-linked pyrrolizine core **50** was acquired via a one-pot 1,3-dipolar cycloaddition process between azomethine intermediates (*in situ* formed from **1** with **6b**) and dipolarophile reagents **49** (Schemes 18). Many of the obtained molecules showed important antiproliferative activities towards the SKNSH tumor cell line. In comparison with doxorubicin (IC_{50} = 6.3 μM), among the **50** products in which $R^1/R^2/R^3$ = OMe/Cl/H and OMe/I/H were the robust actives with IC_{50} values of 4.61 and 5.04 μM, respectively. The authors did not examine the stereochemistry of **50** [30].

As shown in Scheme 19, dipolar cycloaddition between azomethine intermediates (*in situ* generated from **1** with **6**) and dipolarophile reagents **51** yielded the C_3-spirooxindoles-bearing cyclohexanone **52** in moderate yields (60–74 %). In comparison with standard doxorubicin

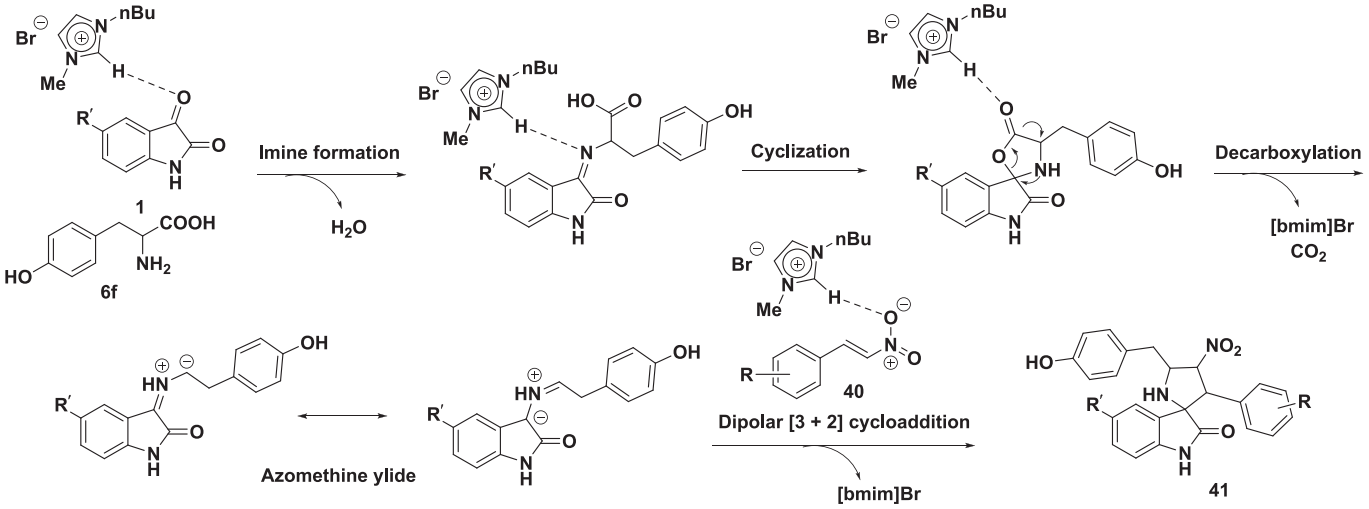

Fig. 9. The proposed mechanism for the construction of **41**.

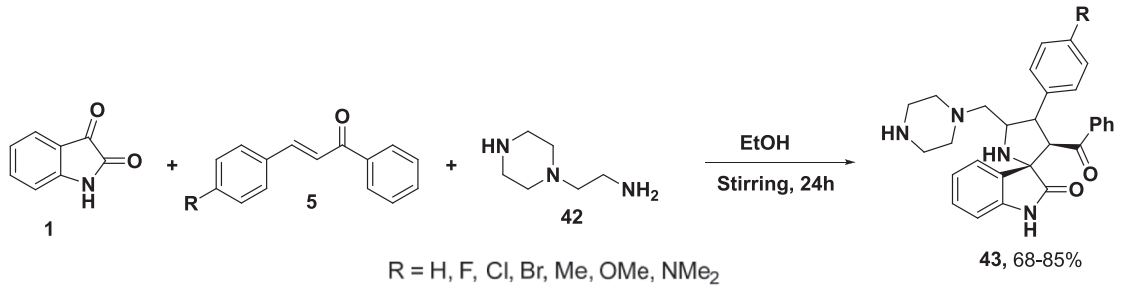

Scheme 15. Chemical construction of C_3-spirooxindoles-linked pyrrolidinone moiety **43**.

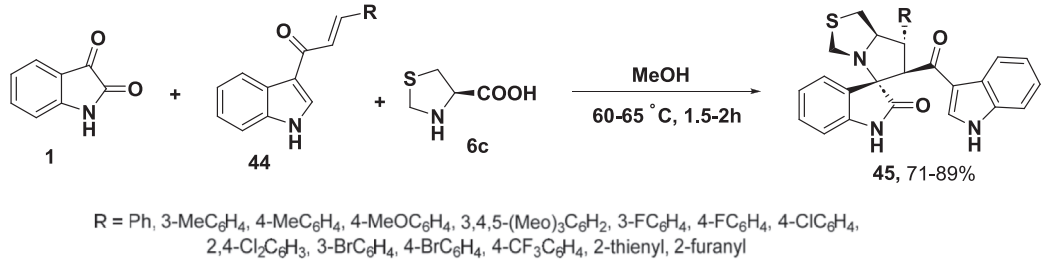

Scheme 16. Chemical construction of C_3-spirooxoindoles-linked thiazolopyrrolidine unit **45**.

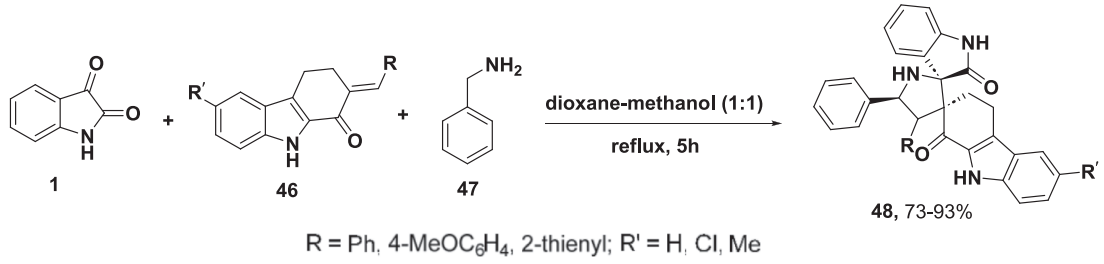

Scheme 17. Chemical construction of C_3-spirooxindole-pyrrolocarbazole hybrids **48**.

(IC_{50} = 0.32–1.9 μM), MTT bioassay results showed that many of the obtained compounds displayed moderate cell growth inhibition activities towards PC3, Hela, and MCF-7, with IC_{50} values ranging from 0.9 to 7.1 μM. The molecular docking study of **52** (R = R' = H) into the active site of MDM2 (PDB ID 1T4E) was performed MOE software v.2019. The best docked pose of **52** (R = R' = H) (-7.20 kcal/mol) showed that the phenyl rings are stabilized into the active pocket through π-π and π-alkyl interactions with amino acid residues, including Leu54, Ile61, Val75, Phe91, Val93, and Ile99. Also, isatin NH and C═O groups form two H-bonds with Leu54 (1.8 Å) and Gly58 (3.4 Å), respectively [31].

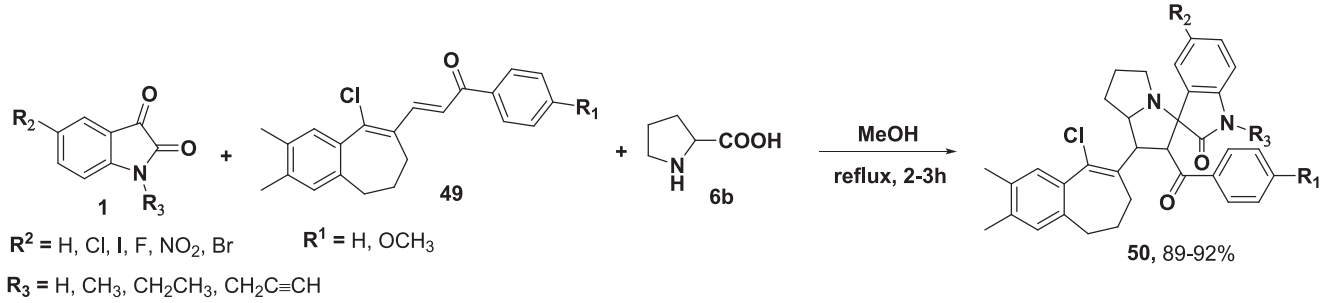

Scheme 18. Chemical construction of C_3-spirooxindole-linked pyrrolizine core **50**.

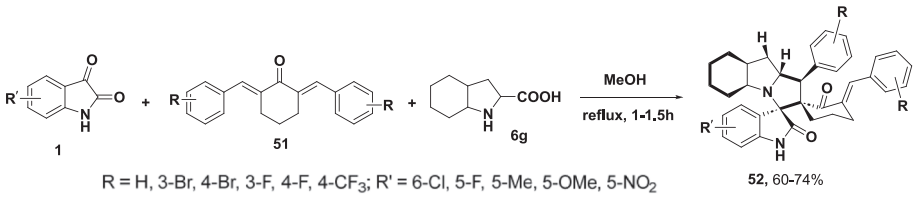

Scheme 19. Chemical construction of C_3-spirooxindole-bearing cyclohexanones **52**.

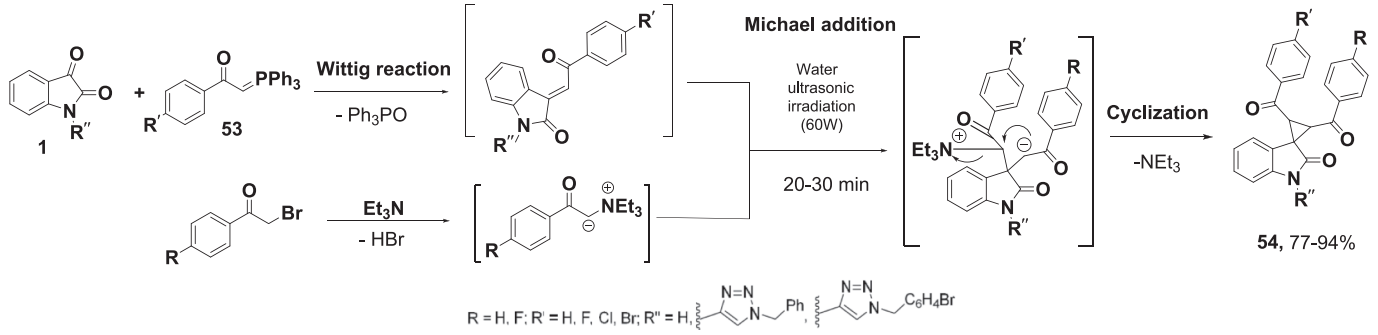

Scheme 20. Chemical construction and the proposed mechanism of C_3-spirooxindoles-linked cyclopropane moiety **54**.

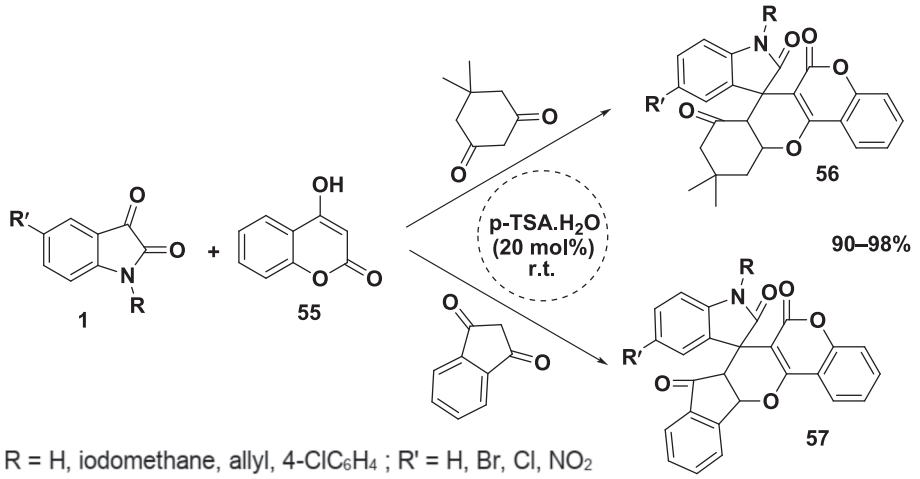

Scheme 21. Chemical construction of C_3-spirooxindoles-bearing coumarin moiety **56** and **57**.

Pourshab's lab in 2019 describes a diastereoselective-green protocol for the sonochemical construction of C_3-spirooxindoles-linked cyclopropane moiety **54** in good to excellent yields (77–94 %) via a two-pot process (Wittig reaction then Michael addition) under aqueous conditions that was mediated by ultrasonic irradiation. Mechanistically, the phenacyltriethylaminium ylide was formed by the nucleophilic attack of triethylamine (*bonding to carbon*) on electrophilic phenacyl bromide, followed by the loss of hydrogen bromide. On the other hand, the Wittig reaction between isatins **1** and phenacylidenetriphenylphosphorane **53** (Wittig reagent) afforded an intermediate dipolarophile. Next, the Michael addition reaction between both intermediates affords a new one that is converted to the final product **54** by a cyclization process and the

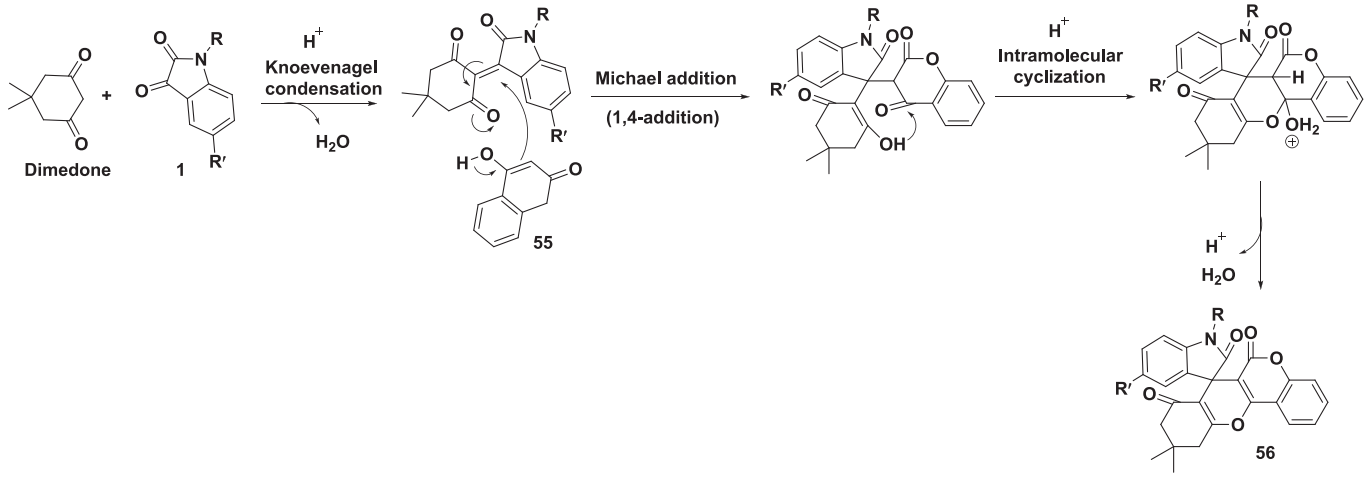

Fig. 10. The proposed mechanism for the construction of **56**.

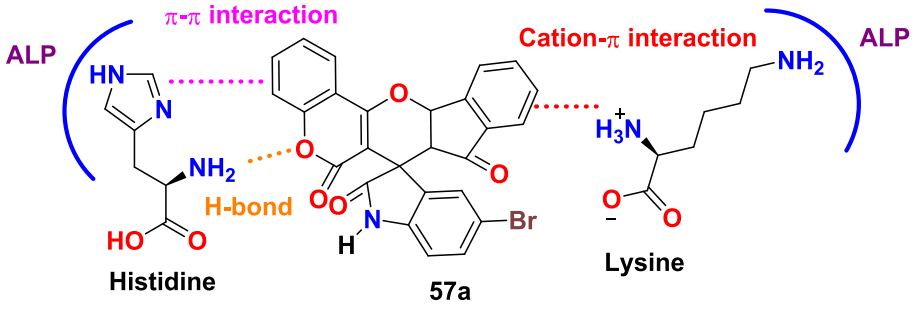

Fig. 11. Main interactions of **57a** with ALP (PDB ID: 2EW2).

loss of the Et_3N molecule (Scheme 20). Many of the installed derivatives showed considerable antiproliferation activities towards HeLa, with IC_{50} values ranging from 4.5 to 12.50 μg/mL (48 h). Among them compound with R/R′/R″ = H/Cl/[1-(4-bromobenzyl)-1*H*-1,2,3-triazol-4-yl] manifested the best cytotoxicity with IC_{50} = 4.50 ± 0.3 μg/mL, while IC_{50} of doxorubicin equals to 1.86 ± 0.1 μg/mL [32].

In 2018, Kumar and his co-authors documented an eco-friendly protocol to construct a library of C_3-spirooxindoles-bearing coumarin moiety **56** and **57**. This condensation process between a three-component mixture composed of **1**, 4-hydroxycoumarin **55**, and active methylene derivatives was aqueous mediated by *p*-toluenesulfonic acid at ambient temperature (Scheme 21). As illustrated in Fig. 10, the formation of **56** was completed via acid-mediated three-step mechanistic pathway, including Knoevenagel condensation, Michael addition (1,4-addition), and intramolecular cyclization followed by removal of water molecule. The *in vitro* cell growth inhibition abilities of the installed compounds were tested towards PC3 and LNCaP cell lines by MTT bioassay. The most effective compounds are **57** that were derived from 5-bromoisatine [**57a**, R = H, R′ = Br; IC_{50} = 0.025 ± 0.002 μM (PC-3)] and *N*-allylisatin [R = allyl, R′ = H; IC_{50} = 1.25 ± 0.09 μM (LNCaP)], while the standard bicalutamide IC_{50} equals to 1.25 ± 0.14 (PC3) and 1.50 ± 0.25 (LNCaP) μM. The interaction mode between **57a** and ALP enzyme (PDB ID: 2EW2) is shown in Fig. 11 via the molecular docking prediction that done by Autodock 4.2.6 and Autodock Tools (ADT) 1.5.6 software. The best docked pose of **57a** details the mechanism of molecular interaction, including H-bonding and noncovalent bonding consisting of π-π and π-cation interactions. The authors did not examine the stereochemistry of **56** and **57** [33].

Also, as a green protocol with solvent-free synthesis, Gobinath *et al.* described the synthesis of C_3-spirooxindoles-linked acridinedione unit **58** via a multicomponent reaction of **1**, 1,3-cyclohexanedione and substituted aniline in the presence of a catalytic amount of *p*-toluenesulfonic acid (Scheme 22). Biologically speaking, many of the installed molecules showed outstanding antiproliferative activities towards MCF-

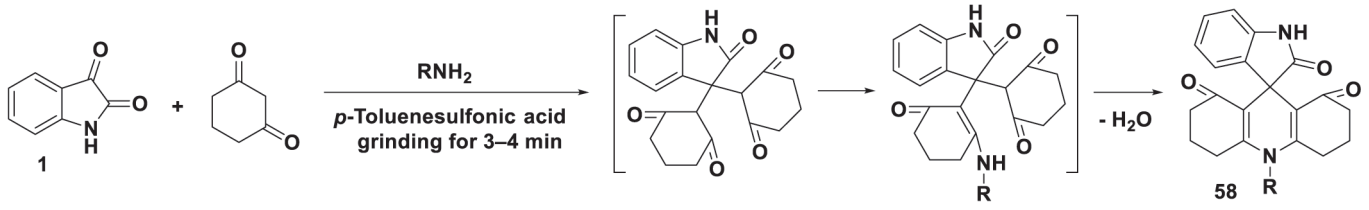

Scheme 22. Chemical construction of C_3-spirooxindoles-linked acridinedione unit **58**.

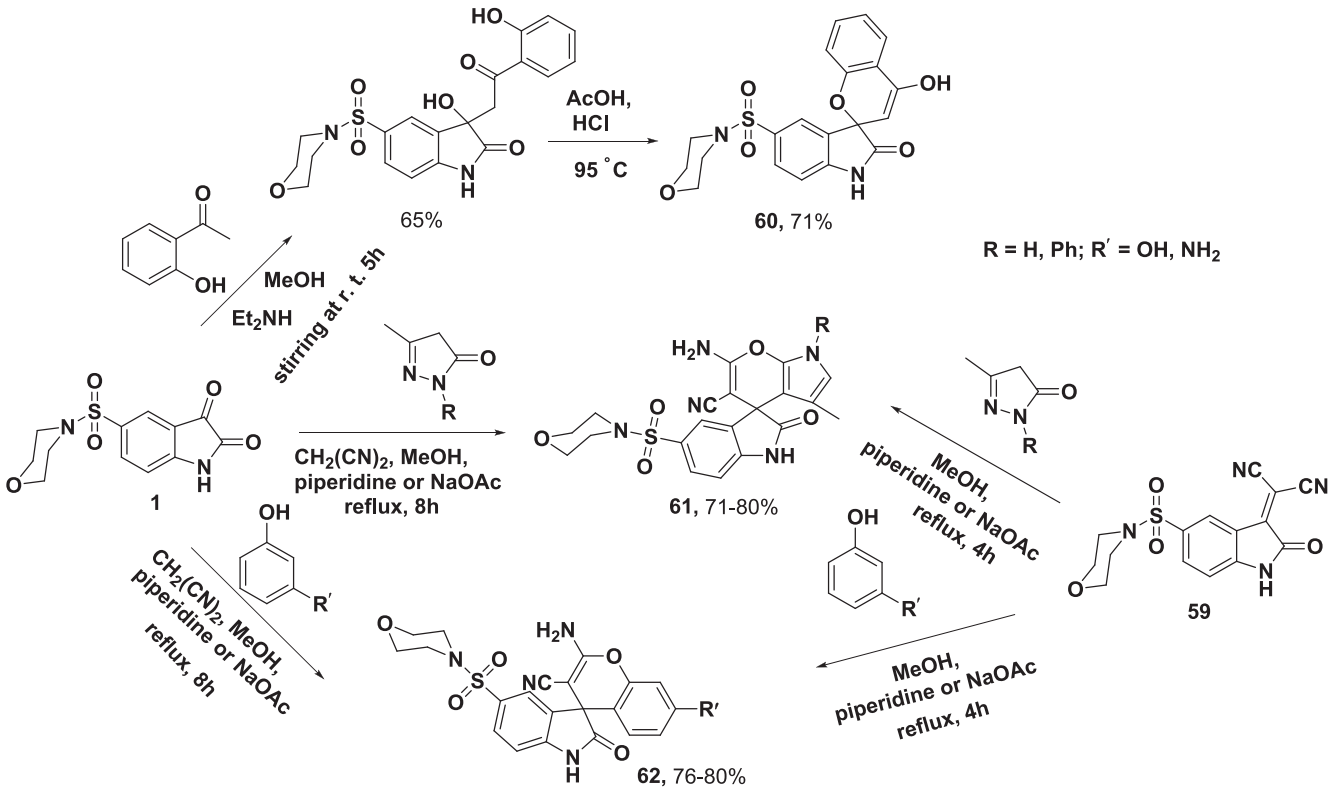

Scheme 23. Chemical construction of C_3-spirooxindoles-linked chromene/pyranopyrrole units **60–62**.

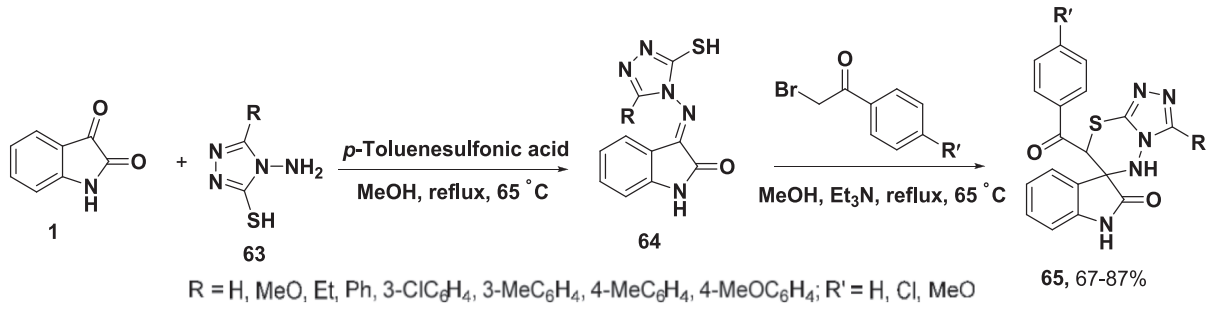

Scheme 24. Chemical construction of C_3-spirooxindoles-bearing triazolothiadiazine unit **65**.

7 via MTT bioassay. Among the **58** products in which R = 4-MeOPh, the robust active one had a GI_{50} (growth inhibitory power) value of 0.01 ± 0.34 relative to the standard doxorubicin 0.02 ± 0.70 μM. The authors did not examine the stereochemistry of **58**, and the isolated yields are not reported [34].

El-Sharief's research group reported a divergent protocol for the construction of C_3-spirooxindoles-linked chromene/pyranopyrrole units **60–62**. Compound **60** was generated via the reaction of **1** and 2′-hydroxyacetophenone in a two-step process, the first was mediated by Et_2NH, and the second cyclization step was completed by AcOH/HCl. Agents **61** and **62** were produced via the reaction of **1** with malononitrile and either pyrazol-5-one or phenols under basic conditions. Another surrogate fashion for the synthesis of **61** and **62** is depicted in Scheme 23. Modest cell growth inhibitory activities were exhibited by the target spirocompounds towards MCF-7, HepG2, and HCT 116 carcinoma cell lines, comparable to doxorubicin. The authors did not examine the stereochemistry of **60–62** [35].

A series of C_3-spirooxindoles-bearing triazolothiadiazine unit **65** was

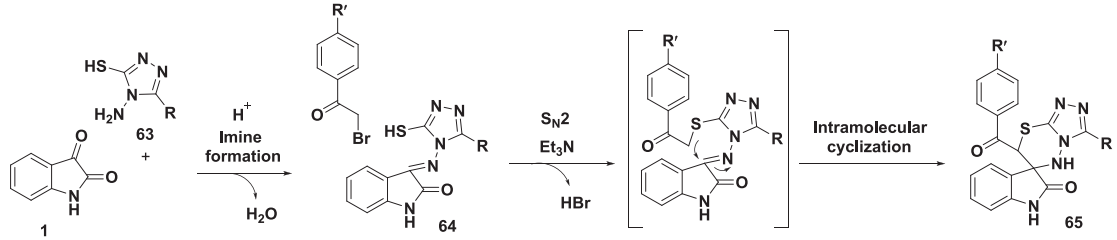

Fig. 12. The proposed mechanism for the construction of **65**.

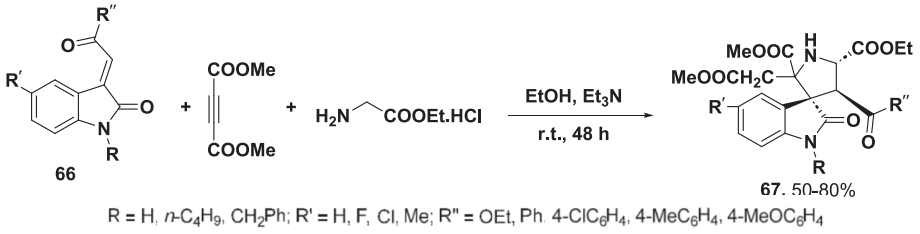

Scheme 25. Chemical construction of C_3-spirooxindoles-based pyrrolidine-linked triester groups **67**.

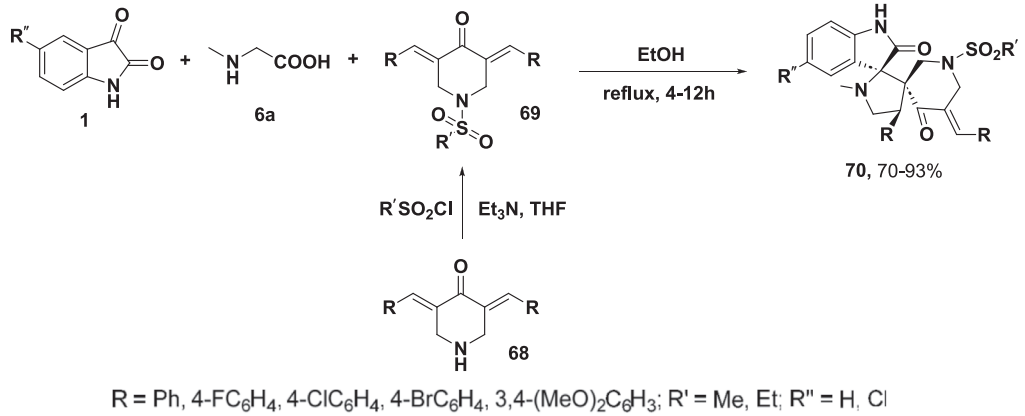

Scheme 26. Chemical construction of C_3-spirooxindoles-based pyrrolidine-linked piperidine **70**.

achieved via a two-step sequential reaction. Firstly, *p*-toluenesulfonic acid (pTSA)-catalyzed the imine formation between **1** and **63** to afford the secondary ketimine **64**. After that S_N2 reaction between electrophilic phenacyl bromides and nucleophilic **64** followed by intramolecular cyclization process afforded **65** in moderate to high yields (Scheme 24, Fig. 12). In comparison with standard 5-fluorouracil [10.38 ± 0.01 (EC109), 24.29 ± 0.04 (DU145), 25.54 ± 0.05 (MGC803), and 22.46 ± 0.03 (MCF-7)], MTT bioassay results showed that many of the installed compounds displayed mild to robust *in vitro* antiproliferative activities. Among them, compound in which R = 4-MePh and R' = H was the most potent one against the tested cell lines [6.62 ± 0.89 (EC109), 8.02 ± 0.64 (DU145), 9.49 ± 0.78 (MGC803), and 17.65 ± 0.82 (MCF-7)]. The authors did not examine the stereochemistry of **65** [36].

The chemical reaction between the ethanolic solution of ylideneoxindoline-2-ones **66** and azomethine ylide that formed from ethyl glycinate hydrochloride and dimethyl acetylenedicarboxylate (DMAD) at room temperature under basic conditions (Et_3N) yielded C_3-spirooxindoles-based pyrrolidine-linked triester groups **67** in moderate to good yields (Scheme 25). MTT bioassay results confirmed that some of the prepared molecules displayed prominent antiproliferative activities towards CT26 and HepG2 tumor cell lines. The compound with R = CH_2Ph, R′ = F, and R″ = 4-MeC_6H_4 at a concentration of 50 μg/mL exhibited cell death % values of 35.39 and 75.15 against HepG2 and CT26, respectively, in 48 h [37].

2.2. Chemical synthesis of antiviral C_3-spirooxindoles

COVID-19 emerged as a global pandemic by WHO in March 2020. COVID-19 is caused by infection with SARS-CoV-2 that affects all the world, leading to millions of people being infected and dying. Consequently, this outbreak has caused global social and economic disruption [38]. A group of C_3-spirooxindoles-based pyrrolidine-linked piperidines **70** were constructed in good to excellent yields (70–93 %) by a regioselective 1,3-dipolar cycloaddition reaction between azomethine intermediates (*in situ* produced from **1** with **6a**) and dipolarophile reagents **69**, which were synthesized through nucleophilic substitution between the corresponding amines **68** and sulfonyl chlorides (Scheme 26). Many of the prepared compounds displayed attractive antiviral activities towards SARS-CoV-2 and considerable safety behavior against the host cell. Among the **70** products in which R = 4-FPh, R' = Et, and R″ = Cl, the robust active one had an IC_{50} value of 7.69 μM and more active than the reference drugs (chloroquine and hydroxychloroquine) with about 3.3 and 4.8 times [38].

Xu *et al.*'s (2019) paper shows the design and the chemical construction of C_3-spirooxindoles-linked triazolopyridine unit **73** via a one-pot two-step reaction of **1**, aminotriazole derivative **71**, and Meldrum's

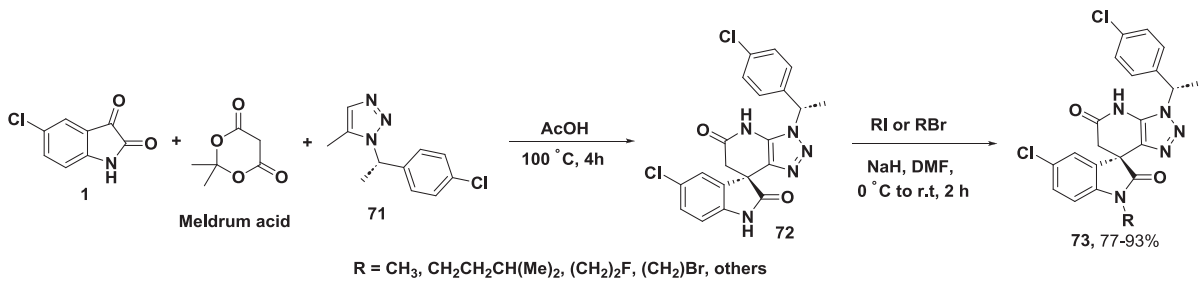

Scheme 27. Chemical construction of C_3-spirooxindoles-linked triazolopyridine unit **73**.

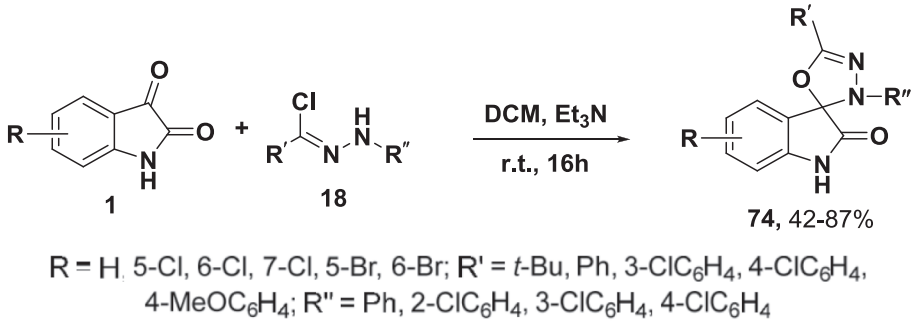

Scheme 28. Chemical construction of C_3-spirooxindoles-linked oxadiazole unit **74**.

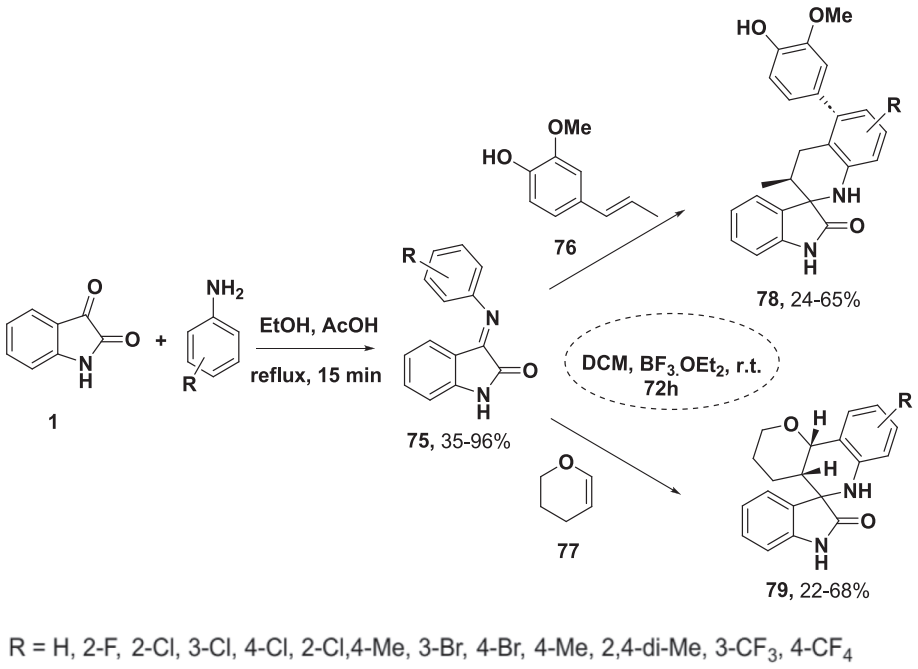

Scheme 29. Chemical construction of C_3-spirooxindoles-linked quinoline unit **78** and **79**.

acid under refluxing acidic conditions, followed by selective *N*-alkylation of the oxindole derivative **72** (Scheme 27). Among the **73** agents in which R = $CH_2CH_2CH(Me)_2$, was the most active one towards DENV-1, −2, and −3 with EC_{50} values of 0.78, 0.16, and 0.035 μM, respectively. Also, the prior molecule demonstrated good *in vivo* pharmacokinetic characteristics and activity in the A129 mouse model, showing its therapeutic promise as a medication candidate for further preclinical research against dengue virus infection [39].

2.3. Chemical synthesis of antimalarial C_3-spirooxindoles

Malaria is one of the world's most prevalent diseases. This is since mosquitoes thrive in tropical and subtropical areas with a high global population. Many parasitic protozoan species that cause this disease have been shown to be transmitted to humans through mosquito bites. Even though numerous malaria agents have been investigated, there is always a need for new ones [40]. Scheme 28 shows the construction of C_3-spirooxindoles-linked oxadiazole unit **74** in moderate to high yield (42–87 %) through nitrilimine cycloaddition generated from dehydrochlorination of hydrazonyl chloride **18** and **1**. Many of the installed spirooxindole agents show outstanding activity towards the erythrocytic stage of *P. falciparum* and the liver-stage of *P. berghei*. This result confirms the possibility of developing potent compounds to suppress both liver-stage (*P. berghei*) and blood-stage (*P. falciparum*) parasites. The

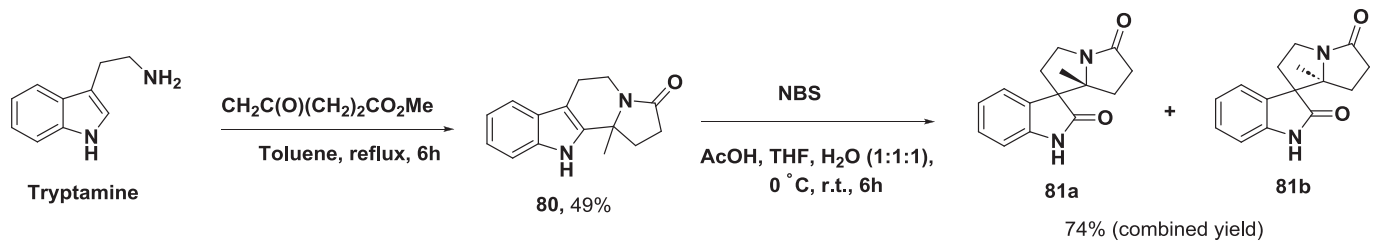

Scheme 30. Chemical construction of C_3-spirooxindoles-linked indolizine unit **81a** and **81b**.

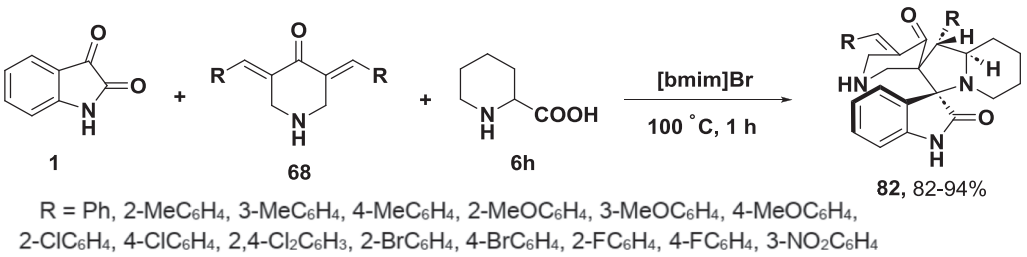

Scheme 31. Chemical construction of C_3-spirooxindoles-based indolizine-linked piperidone unit **82**.

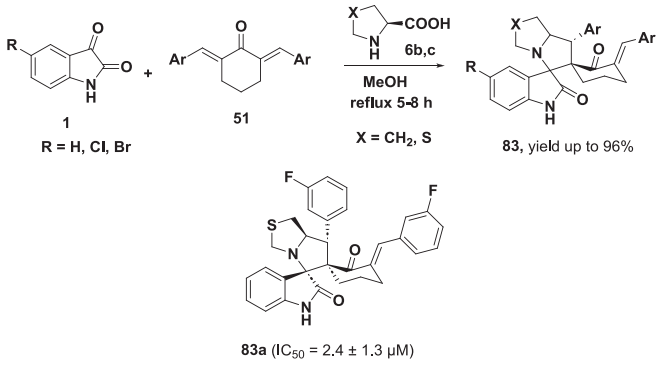

Scheme 32. Chemical construction of C_3-spirooxindoles-containing benzylidene indolines **83**.

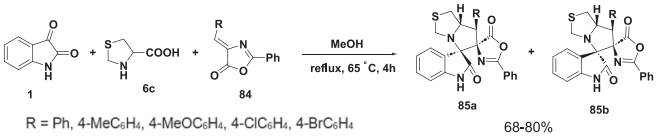

Scheme 33. Chemical construction of C_3-spirooxindoles-containing oxazolone moiety **85a**,**b**.

authors did not examine the stereochemistry of **74** [41].

Mathebula research group (2019) reported the construction of C_3-spirooxindoles-linked quinoline unit **78** and **79** via $BF_3.OEt_2$-catalyzed Povarov reaction of isatin-derived imines **75** and alkenes **76** or **77**, respectively (Scheme 29). In comparison with chloroquine [$IC_{50} = 0.110 \pm 0.002$ (FCR − 3) and 0.0127 ± 0.003 (3D7) μM], several of the compounds **78** showed *in vitro* antiplasmodial efficacy against *P. falciparum* drug-resistant FCR-3 and *P. falciparum* drug-sensitive 3D7 strains with IC_{50} values of 1.52–4.20 and 1.31–1.80 μM, respectively [42].

Scheme 30 displays the chemical construction of C_3-spirooxindoles-linked indolizine unit **81a** and **81b** via the reaction of **80** with *N*-bromosuccinimide in an acidic solvent system at 0 °C, raised to the ambient temperature. The installed compounds showed moderate antiplasmodial activities towards the artemisinin-sensitive (3D7) and resistant *P. falciparum* strains (R539T) with IC_{50} ranging from 2.99 to 4.89 μM after 48 h [43].

2.4. Chemical synthesis of anti-inflammatory C_3-spirooxindoles

The research work of Kumar *et al.* (2018) indicates the construction of C_3-spirooxindoles-based indolizine-linked piperidone unit **82** through a stereoselective one-pot 1,3-dipolar cycloaddition reaction between azomethine intermediates (*in situ* produced from **1** and pipecolinic acid **6 h**) with dipolarophile reagents **68** in ionic liquid [bmim]Br (Schemes 31). Several of the produced compounds manifested pivotal anti-inflammatory activities comparable to indomethacin, with inhibitory observations towards PGE2, TNF-*α*, and nitrite levels [44].

As a common synthetic protocol, C_3-spirooxindoles-containing benzylidene indolines **83** were chemically constructed through a one pot [3 + 2] cycloaddition reaction between azomethine intermediates (*in situ* produced from **1** with **6b,c**) and dipolarophile chalcones-based cyclohexanone **51** (Scheme 32). In comparison with ibuprofen ($IC_{50} = 11.2 \pm 1.9$ μM), C_3-spirooxindole **83a** that contains fluorobenzene units (R = H, Ar = 3-FC_6H_4) displayed the best *in vitro* anti-inflammatory activity with IC_{50} value of 2.4 ± 1.3 μM. The docking study of **83a** towards the murine cyclooxygenase-2 (COX-2, PDB ID 4PH9) was carried out by MOE v2018.0101. The study showed the importance of fluorobenzene units. One among them is interacted with the binding site via non-polar contacts with amino acid residues consisting of Leu532, Leu535, Val345, and Val350. While the other one displays a π-π *T*-shaped interaction with Tyr356. Also, two H-bonds are formed between the ligand and the target protein via Val542 and Ala528 [45].

2.5. Chemical synthesis of antidiabetic C_3-spirooxindoles

Still with the common protocol, C_3-spirooxindoles-containing oxazolone moiety **85a**,**b** were designed and installed in moderate to good yields (68–80 %) as a mixture of two diastereoisomers via a MCR 1,3-dipolar cycloaddition reaction between azomethine intermediates (*in situ* produced from **1** and **6c**) with dipolarophile 4-arylidene-5(4*H*)-oxazolones **84** (Scheme 33). Biologically, in comparison with acarbose [$IC_{50} = 1.28 \pm 0.13$ (HAA) and 2.80 ± 0.20 μM (SCAG)], compound **85a** with R = 4-MePh was the most active antihyperglycemic agent towards *α*-amylase (HAA) and *α*-glucosidase (SCAG) with IC_{50} values of 1.76 ± 0.14 and 4.81 ± 0.24 μM, respectively [46].

Toumi *et al.*'s (2021) study represents the creation of C_3-spirooxindoles-linked pyrrolidine-fused rhodanine heterocycle **87** in moderate to excellent yields (66–96 %) via a MCR 1,3-dipolar cycloaddition reaction between azomethine intermediates (*in situ* produced from **1** and glycine methyl ester) with dipolarophile reagents **86** (Scheme 34). The synthesized compounds display high *α*-amylase suppression with IC_{50} values ranging from 1.49 ± 0.10 to 3.06 ± 0.17 μM, comparable to acarbose ($IC_{50} = 1.56 \pm 0.07$ μM) [47]. The most active agents, **87a**, **87b**, **87c**, and **87d**, were tested *in vivo* for hypoglycemic characteristics in alloxan-induced diabetic rats, resulting in a decrease in blood glucose levels. The molecular docking simulation of the most potent inhibitor (**87a**) was applied by MOE v2010.10 against the porcine α-amylase enzyme (PDB code: 1OSE). The thiazolidine C═O and NH groups form H-bonds with His305. The aromatic phenyl groups of **87a** are stabilized within the active site of 1OSE through σ-π-interactions with the Leu162 and Trp59. Also, pyrrolidine NH is interacted with Asp300 via an anionic interaction [47].

In 2022, Nivetha and co-workers published an article that documents the creation of C_3-spirooxindoles-linked pyrrolidine **89**/pyrrolizidine **90** via a stereoselective MCR 1,3-dipolar cycloaddition between azomethine intermediates (*in situ* produced from **1** with **6a,b**) and dipolarophile reagents **88** (Scheme 35). The anti-diabetic properties of spirooxindoles **89** and **90** were screened towards the *α*-glucosidase and α-amylase enzymes. In comparison with acarbose [$IC_{50} = 30.05 \pm 0.05$

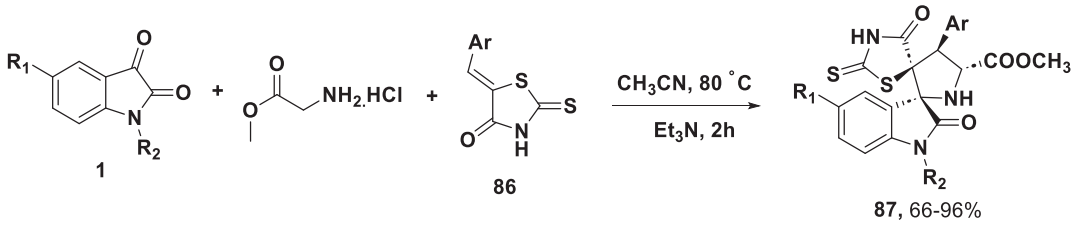

Cpd. No.	R_1	R_2	Ar
87a	Br	H	Ph
87b	Br	H	4-BrPh
87c	NO_2	H	4-BrPh
87d	Br	H	4-ClPh

Scheme 34. Chemical construction of C_3-spirooxindoles-linked pyrrolidine-fused rhodanine heterocycle **87**.

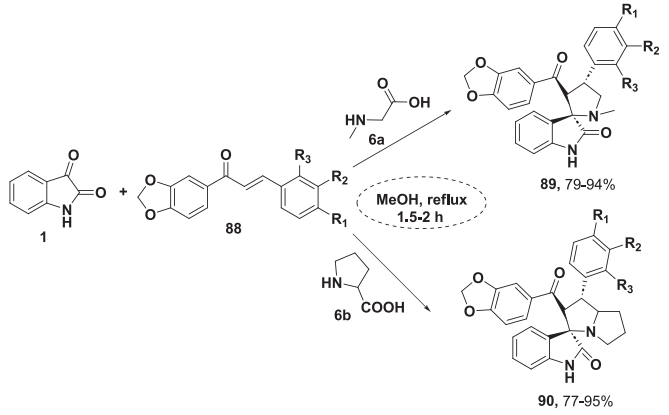

Scheme 35. Chemical construction of C_3-spirooxindoles-linked pyrrolidine **89**/pyrrolizidine **90**.

(α-amylase) and 10.15 ± 0.06 μg/mL (α-glucosidase)], molecule **90a** ($R_1 = R_3 = H$, $R_2 = F$) was the promising one with an inhibition potency towards *α*-glucosidase (IC_{50} = 10.00 ± 0.16 μg/mL) and α-amylase enzymes (IC_{50} = 32.40 ± 0.86 μg/mL). Also, **90a** was docked with α-glucosidase with binding affinity of −10.1 Kcal/mol comparable to acarbose (-8.6 Kcal/mol). The best docking mode shows H-bond interactions between **90a** framework and His279, Arg312, and Phe157. Furthermore, **90a** forms electrostatic interactions with His279 and Glu304. Moreover, **90a** produces a variety of hydrophobic interactions (π-π, σ-π, π-alkyl, and alkyl-alkyl) with many amino acid residues, confirming the robust inhibitory activity of **90a** [48].

Teja and his group in 2020 reported the synthesis of C_3-spirooxindoles-linked pyrrolizine **92**/pyrrolidine **93** through a regioselective sequential manner using Cu–TEMPO that catalyzed the oxidation of ketones **91**, followed by a cycloaddition reaction with azomethine intermediates (*in situ* produced from **1** with **6a,b**) (Scheme 36). The plausible mechanism was reported. Biochemically, in comparison with acarbose [IC_{50} = 0.058 ± 0.012 (α-amylase) and 0.046 ± 0.023 μg/mL (α-glucosidase)], molecule **92a** displayed the best inhibition potency towards α-glucosidase with an IC_{50} value of 0.24 ± 0.05 μg/mL, while **92b** was the best one against α-amylase (IC_{50} = 0.28 ± 0.07 μg/mL). Consequentially, **92a** and **92b** are active at low μg/mL concentrations and could be promising antidiabetic lead candidates [49].

2.6. Chemical synthesis of antimicrobial C_3-spirooxindoles

Under ultrasonic conditions, Gul and his co-researchers (2023) successfully synthesized C_3-spirooxindoles-linked quinoline **97**/pyrazolo [3,4-*b*]quinoline **98** through a MCR including 1, naphthalene-1-amine (**95**)/or 5-amino-1-methyl-3-pheylpyrazole (**96**), and active methylene reagents (**94**). The reaction was mediated by the (±)-camphor-10-sulfonic acid as an organocatalyst (Scheme 37). Biologically speaking, the MIC values of the most active antimicrobial compounds towards *Enterococcus faecalis*, *Staphylococcus aureus,* and *Candida albicans* ranged from 375 to more than 6000 μg/mL relative to gentamicin (4 to > 256 μg/mL) and fluconazole (32 μg/mL). The authors did not examine the stereochemistry of **97** and **98** [50].

Pandey and his co-researchers (2022) reported the creation of the C_3-spirooxindoles-linked cyclopropane moiety **100a–e**. These hybrids were installed in excellent yields (91–94 %) via a MCR of methyleneindolinones **66** with the aromatic aldehydes and $TsNHNH_2$ in the presence of K_2CO_3. Compound **66** was prepared by a Wittig reaction of **1** with Wittig reagent **99** (Scheme 38). Nucleophilic addition reaction between aldehydes and $TsNHNH_2$ gives the corresponding hydrazones that converted by K_2CO_3 to the dipolarophile aryldiazo-methane via removal of tosyl group. Then [3 + 2] cycloaddition with Wittig product **66** and removing of N_2 molecule afforded the desired molecules **100** (Fig. 13) [51]. Comparable to Scheme 20 [32], S_N2 reaction between phenacyl bromides and nucleophilic Et_3N yielded the corresponding dipolarophile that converts to the final products **54** via Michael addition reaction with Wittig products [32]. Biologically, in comparison with ciprofloxacin (MIC = 0.007–3.9 μg/mL), compound **100d** with R = Br and Ar = 3-C_6H_4-O-CH_2-Ph showed vital antimicrobial activities towards Gram-positive and modest activity against Gram-negative pathogenic bacteria, with MIC values ranging from 0.007 to 7.88 μg/mL [51].

Conventionally, Salem *et al.* (2020) demonstrated the chemical creation of C_3-spirooxindoles-linked pyran unit **101** and **102**. These target molecules were generated via a two-step process started by the Knoevenagel condensation reaction of **1** and malononitrile/ethyl cyanoacetate, followed by the Michael 1,4-addition reaction between Michael acceptor **59** and 1,3-dicarbonyl Michael donors (*β*-ketoester/*β*-diketone) to afford the desired Michael adducts **101** and **102** (Scheme 39). Several of the installed molecules showed optimistic antimicrobial activities. Among them, molecules **101f,h**, and **102a,c,e,f,g** were the robust agents towards *S. aureus* with significant gyrase suppression activities, with IC_{50} values ranging from 18.07 to 27.03 μM relative to ciprofloxacin (26.43 μM). The authors did not examine the stereochemistry of **101** and **102** [52]. The docking study was carried out by the MOE v2008.10 towards the DNA gyrase (PDB ID: 2XCT). The best binding affinity was achieved by **102c** (-19.73 kcal/mol) comparable to ciprofloxacin (-11.87 kcal/mol). The oxygen atom of the morphinyl unit forms a H-bond with Ser1028 (2.58 Å), while the isatin NH generates another one with Ala509 (3.07 Å). The third one was formed between pyran NH_2 and Tyr580 (2.84 Å), proving the reactivity of **102c** [52].

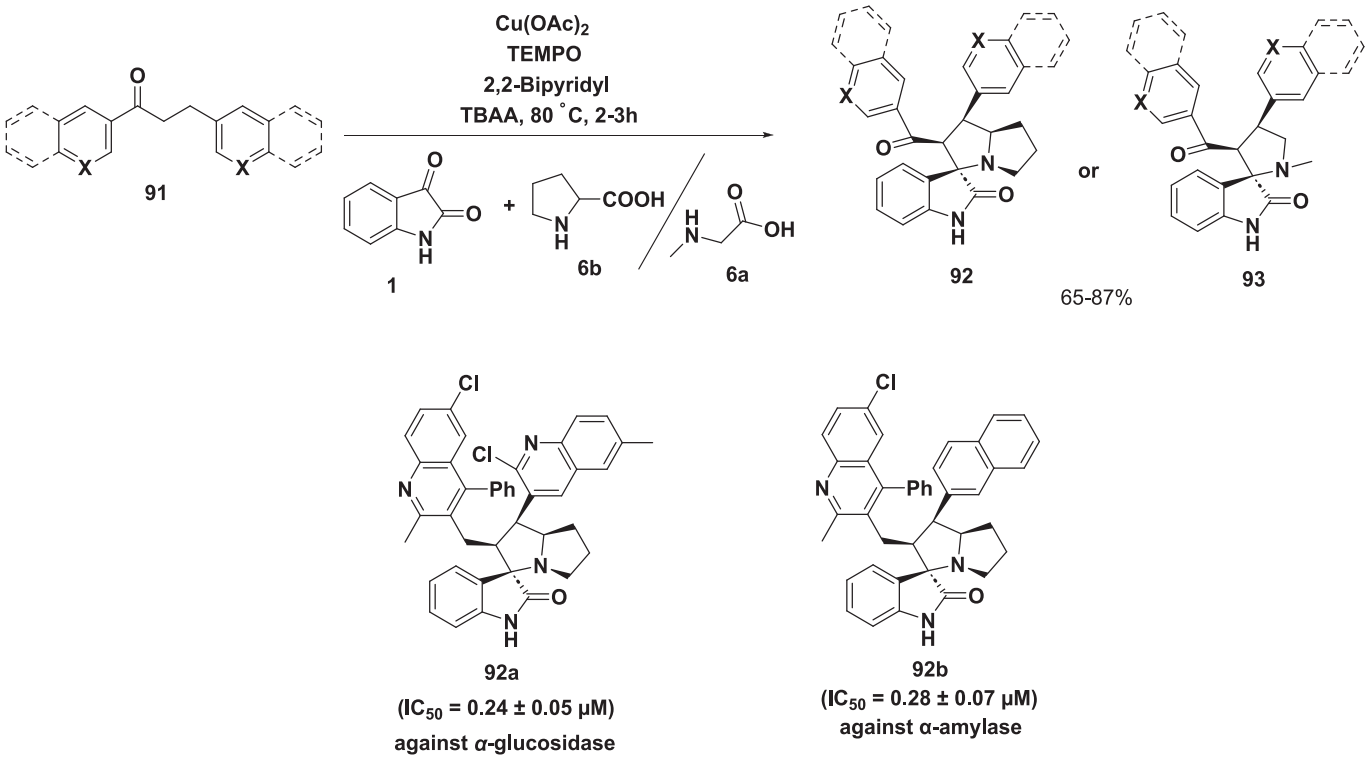

Scheme 36. Chemical construction of C_3-spirooxindoles-linked pyrrolizine **92**/pyrrolidine **93**.

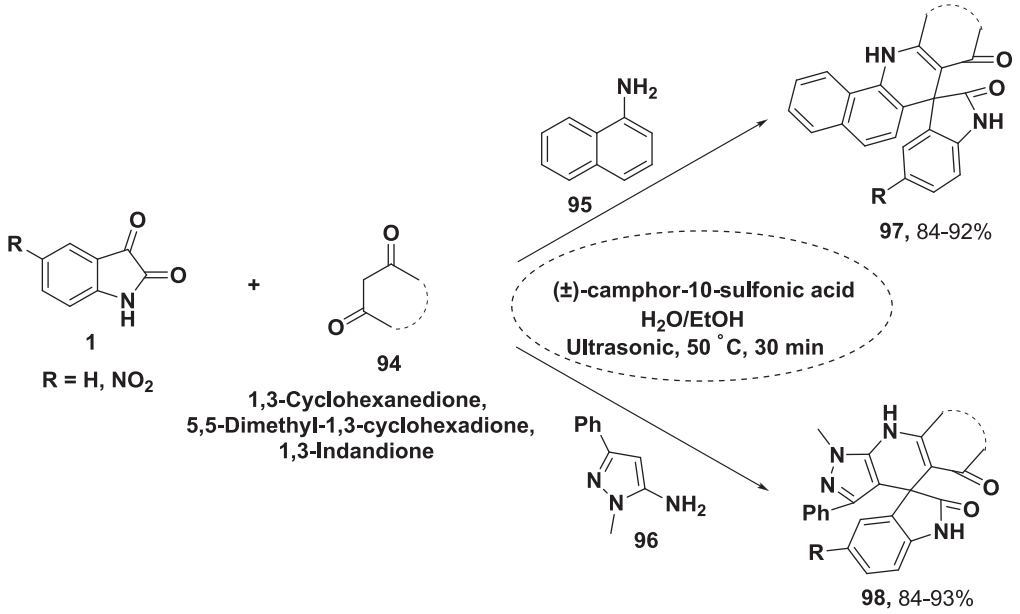

Scheme 37. Chemical construction of C_3-spirooxindoles-linked quinoline **97**/pyrazolo[3,4-*b*]quinoline **98**.

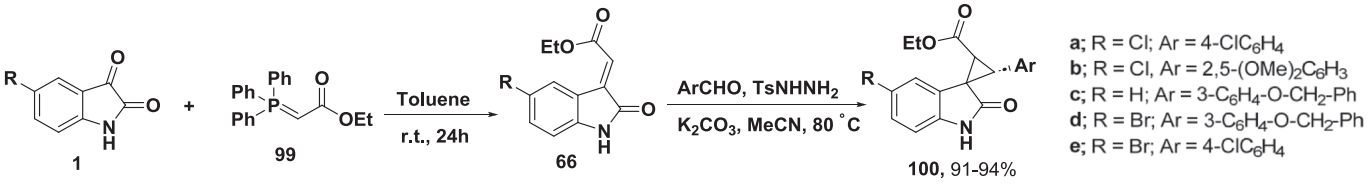

Scheme 38. Chemical construction of C_3-spirooxindoles-linked cyclopropane moiety **100a–e**.

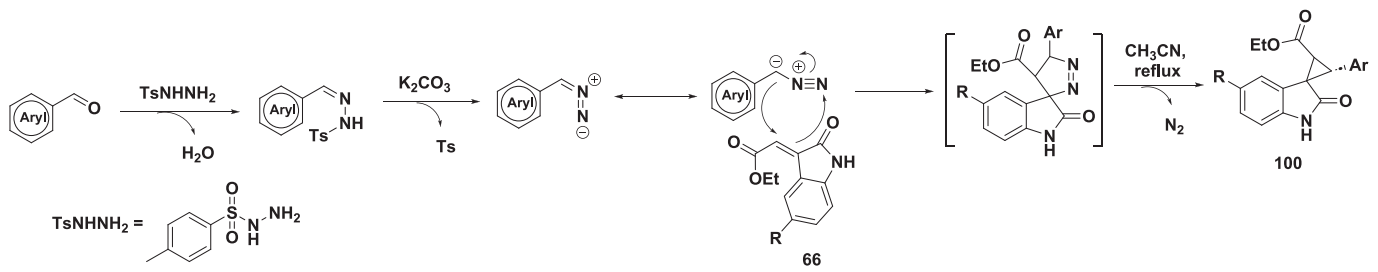

Fig. 13. The proposed mechanism for the construction of **100**.

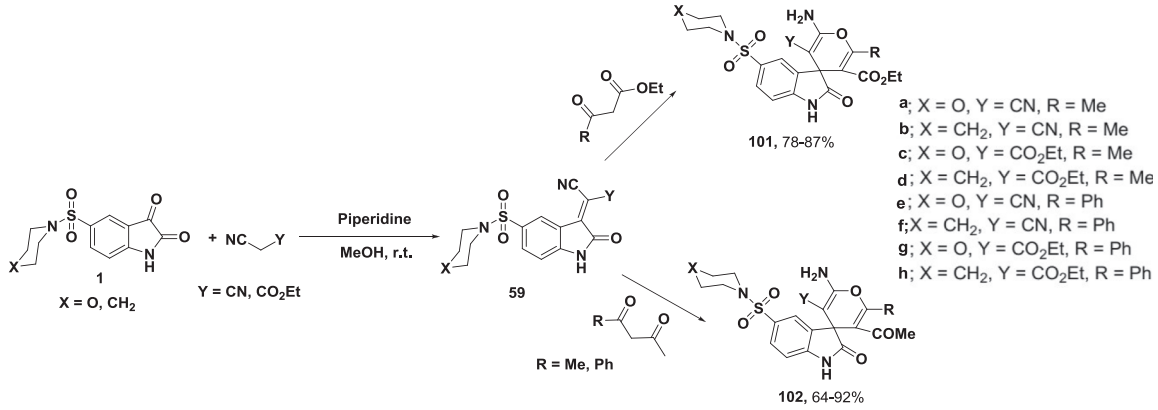

Scheme 39. Chemical construction of C_3-spirooxindoles-linked pyran unit **101** and **102**.

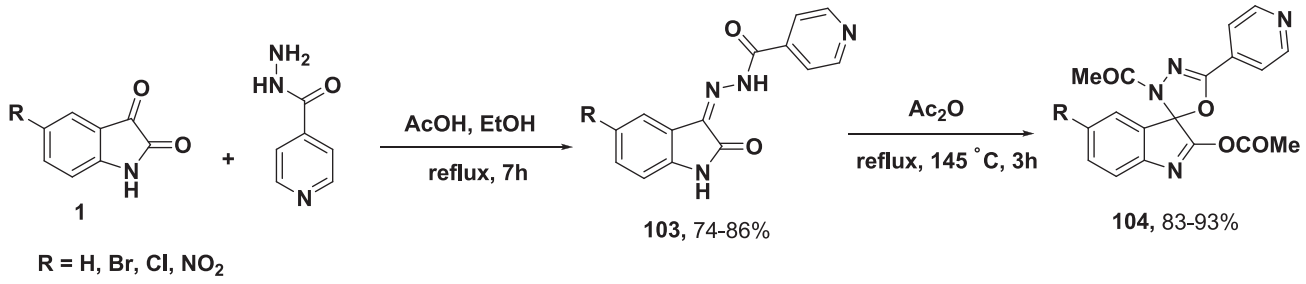

Scheme 40. Chemical construction of C_3-spirooxindoles-linked oxadiazol unit **104**.

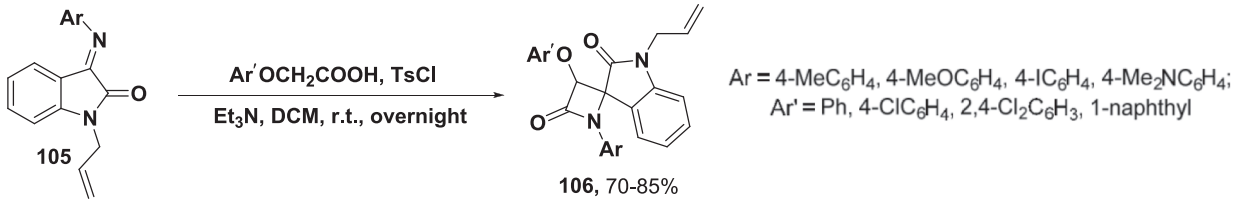

Scheme 41. Chemical construction of C_3-spirooxindoles-linked β-lactam unit **106**.

Also, in the traditional pathway, Nalini *et al.* (2022) described the chemical creation of C_3-spirooxindoles-linked oxadiazol unit **104** via a two-step process that began with hydrazide-hydrazone formation **103** and was followed by cyclization with acetic anhydride to furnish the target compounds **104** (Scheme 40). Good antimicrobial activities were observed for the installed molecules. Among the **104** products in which R = Cl, the robustly active one towards *B. subtilis* and *E. coli* had a MIC value of 12.5 μg/mL (equipotent with Gentamicin). Also, the most potent anti-mycobacterial agents in which R = Br or Cl had an IC_{50} value of 6.25 μg/mL. The authors did not examine the stereochemistry of **104** [53].

C_3-Spirooxindoles-linked β-lactam (Scheme 41) unit **106** were generated via a [2 + 2] cycloaddition of isatin-derived imines **105** with aryloxy acetic acid (Scheme 42). The prepared molecules showed low antibacterial activities (MIC > 200 μM) towards *S. aureus*, *E. coli*, and *P. aeruginosa*. Also, the authors reported the antimalarial activities of these compounds, **106b** (Ar = 4-MePh, Ar' = 2,4-Cl_2Ph) was the robust one against *P. falciparum* K1 Strain with IC_{50} value of 5.04 ± 0.28 μM comparable to chloroquine (IC_{50} = 0.80 μM). The authors did not examine the stereochemistry of **106** [54].

Also traditionally, the Radwan research group (2022) documented the chemical formation of C_3-spirooxindoles-linked pyrazoline unit

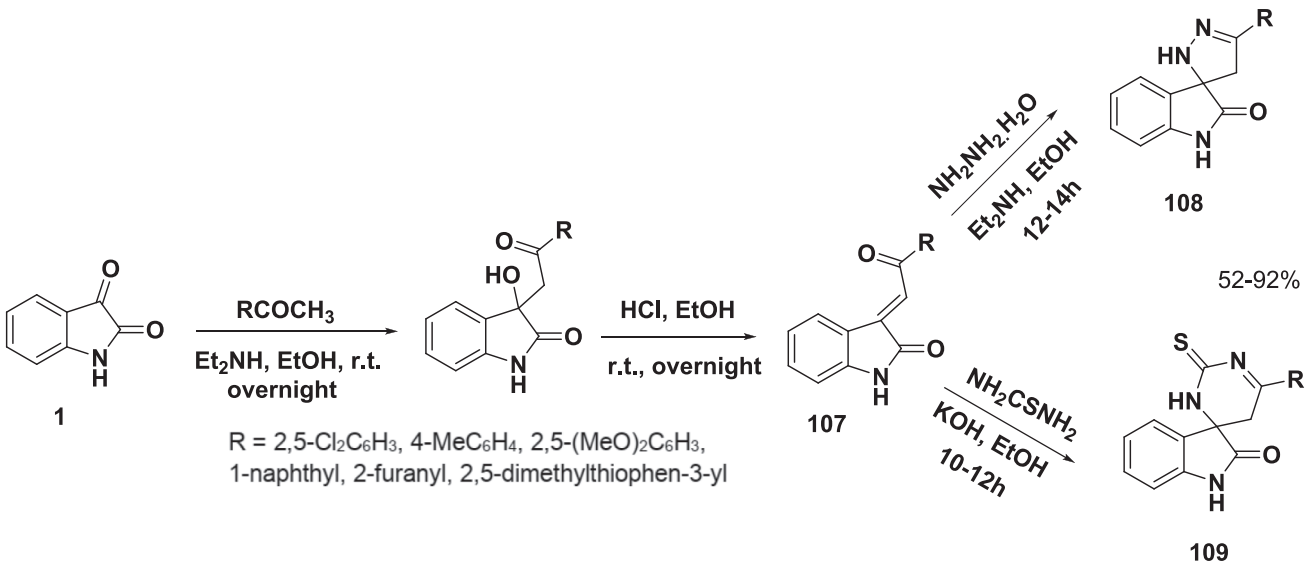

Scheme 42. Chemical construction of C_3-spirooxindoles-linked pyrazoline unit **108**/pyrimidine unit **109**.

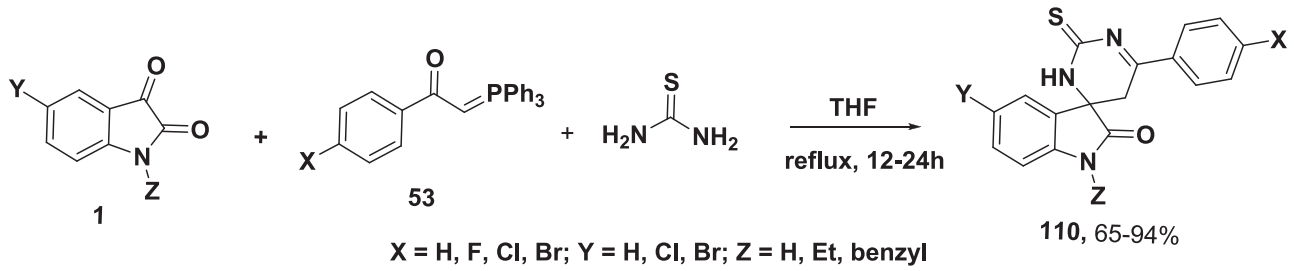

Scheme 43. Chemical construction of C_3-spirooxindoles-linked pyrimidine core **110**.

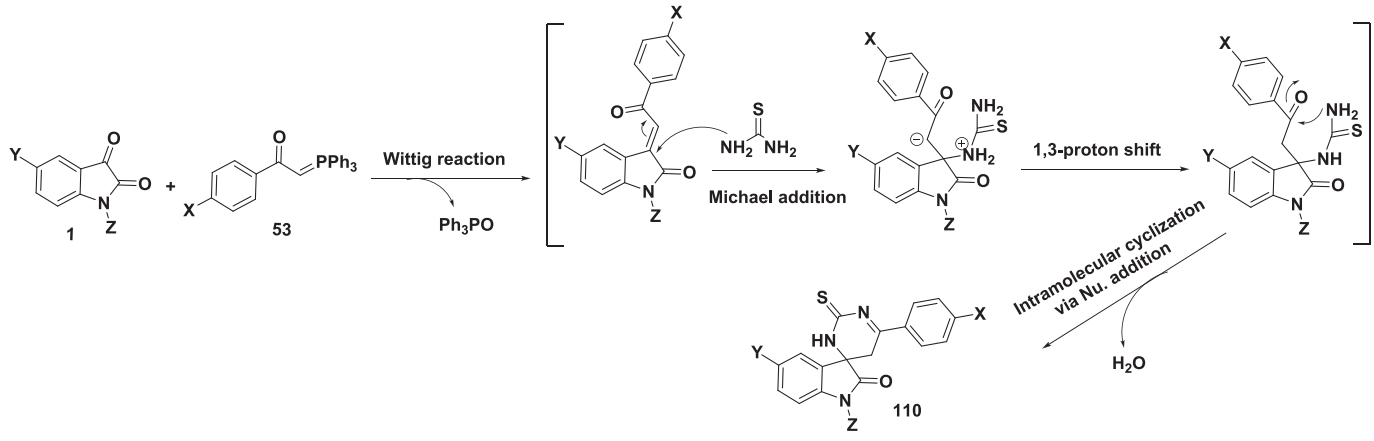

Fig. 14. The proposed mechanism for the construction of **110**.

108/pyrimidine unit **109** in moderate to excellent yields (52–92 %) via a two-step process started by an Et_2NH-promoted nucleophilic addition reaction between **1** and acetophenones, followed by catalytic dehydration to produce **107**. The second step was completed through the basic cyclization of **107** with hydrazine hydrate and thiourea to afford **108** and **109**, respectively (Scheme 42). In comparison with imipenem (MIC = 0.026 mmol/L), the created molecules displayed optimistic antibacterial activities towards *B. subtilis* and *S. aureus*, with MIC values of 0.348–1.809 and 0.044–0.226 mmol/L, respectively. The authors did not examine the stereochemistry of **108** and **109** [55].

In the same fashion, Pourshab *et al.* (2018) successfully published the formation of C_3-spirooxindoles-linked pyrimidine core **110** via a MCR of **1**, Wittig reagent **53**, and thiourea. The process seems to proceed through the Wittig reaction between **1** and **53**, followed by the Michael addition on C_β between the Wittig product and thiourea. After that, sequential 1,3-proton shift, and intramolecular cyclization via nucleophilic addition of the installed intermediates afforded the desired products **110** (Scheme 43, Fig. 14). Antimicrobial inspection manifested that the agent with X/Y/Z = F/Cl/H was the most promising one towards *S. aureus*, *B. subtilis*, *E. coli*, and *P. aeruginosa,* with inhibition zone

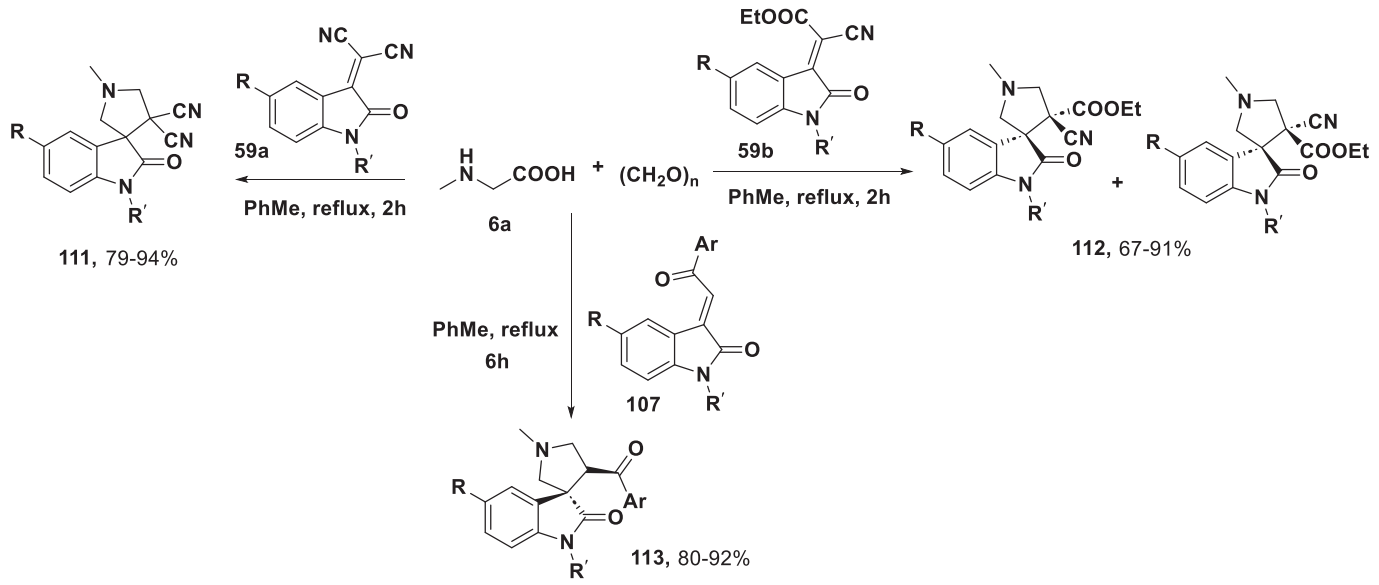

Scheme 44. Chemical construction of C_3-spirooxindoles-linked pyrrolidine moiety **111**–**113**.

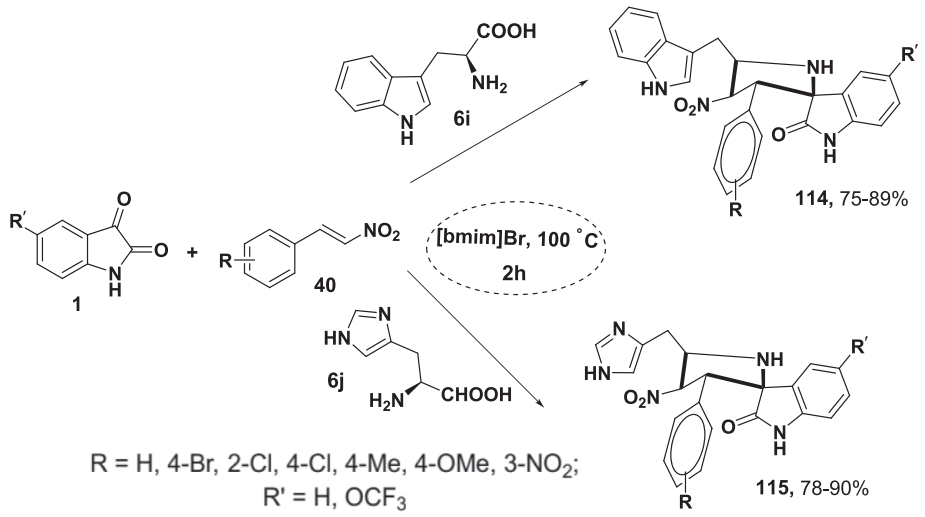

Scheme 45. Chemical construction of C_3-spirooxindoles-linked nitropyrrolidine unit **114** and **115**.

values of 13.5, 14.0, 8.5, and 9.0 mm, respectively, comparable to the gentamicin reference drug (inhibition zone = 20.3, 26.0, 19.6, and 15.6 mm, respectively). The authors did not examine the stereochemistry of **110** [56].

In 2018, Huang *et al.* reported the chemical creation of a new C_3-spirooxindoles-linked pyrrolidine moiety **111**–**113** via a one-pot [3 + 2] cycloaddition reaction between Knoevenagel condensation products **59a,b**, and azomethine intermediates (*in situ* installed from **6a** and

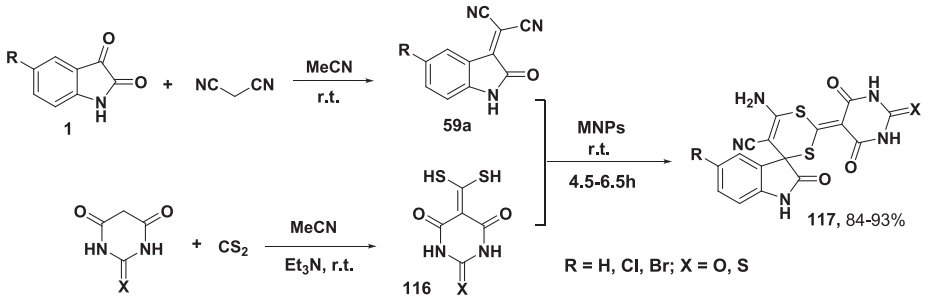

Scheme 46. Chemical construction of C_3-spirooxindoles-linked dithiine fragment **117**.

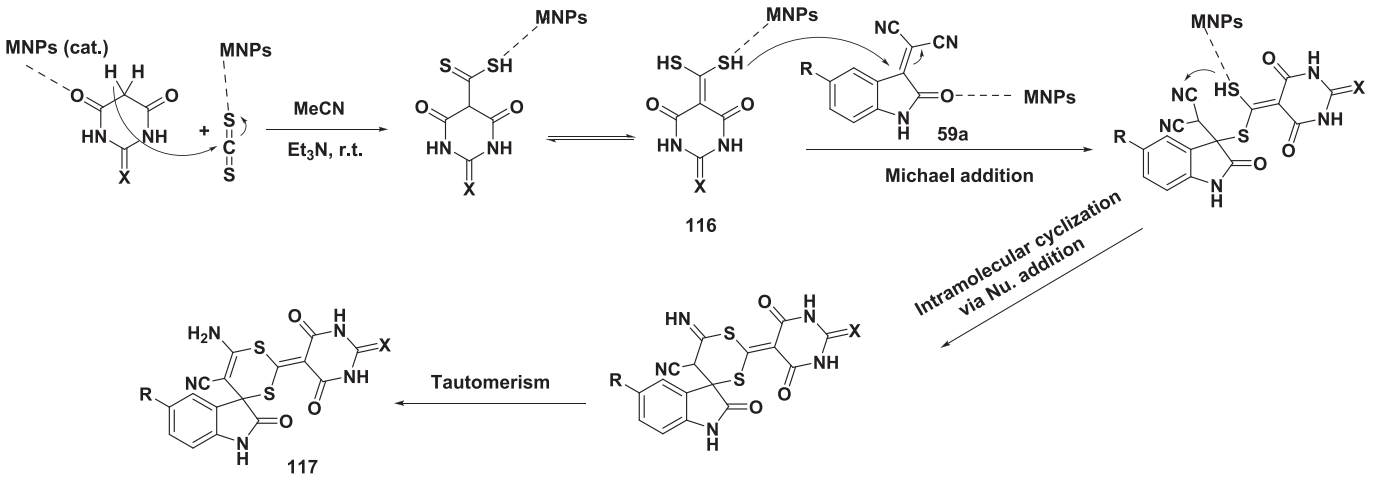

Fig. 15. The proposed mechanism for the construction of **117**.

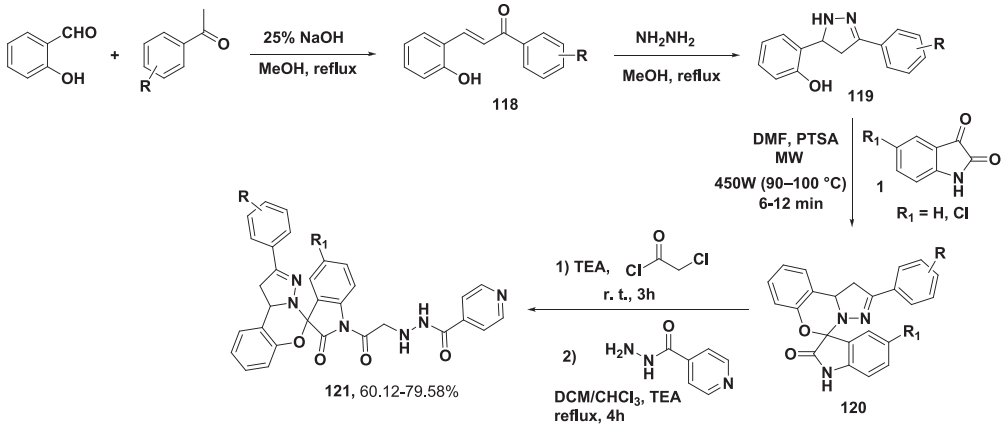

Scheme 47. Chemical construction of C_3-spirooxindoles-linked isoniazid unit **121**.

paraformaldehyde) (Scheme 44). Biologically, moderate to low antibacterial activities were observed by some of the prepared compounds towards *S. aureus* and *E. coli*, with MIC values ranging from 250 to 1000 μg/mL [57].

In the same manner as the synthesis of anticancer C_3-spirooxindole-pyrrolidine heterocyclic hybrids **41**, a set of spirooxindoles-linked nitropyrrolidine unit **114** and **115** was achieved in high isolated yields (75–90 %) by [bmim]Br-promoted [3 + 2] cycloaddition of a MCR between azomethine intermediates [*in situ* installed from **1** with L-tryptophan (**6i**) or L-histidine (**6j**)] and dipolarophile reagent **40** (Scheme 45). The authors also screened the antifungal activity, which showed compounds **114** were most potent towards *C. albicans*, with MIC values ranging from 4 to 128 μg/mL through biofilm degradation [58].

The work of Moghaddam-Manesh *et al.* (2020) describes the creation of C_3-spirooxindoles-linked dithiine fragment **117** via nucleophilic cycloaddition of **116** and Knoevenagel condensation products **59a**. The reaction was assisted by heterogenous magnetic nanoparticles (Fe_3O4@gly@CE, MNPs) as a recyclable catalyst (Scheme 46). Mechanistically, Et_3N-catalyzed the reaction between carbon disulfide and barbituric acid (or thiobarbituric acid) to yield **116**, which reacts with Knoevenagel product **59a** via Michael addition pathway followed by intramolecular cyclization and then tautomerism to generate the final products **117** (Fig. 15). Several of the installed compounds showed a good antimicrobial profile. Among them, the agent in which R = Cl and X = O, was the most potent one towards *A. fumigatus* and *C. albicans*, with a MIC value of 8 μg/mL. The authors did not examine the stereochemistry of **117** [59].

In 2020, Borad *et al.* documented the chemical creation of C_3-spirooxindoles-linked isoniazid unit **121** via a multi-step protocol that started with the formation of pyrazole derivative **119** via a hydrazinolysis reaction of α,β-unsaturated compound **118**. Next, the cascade nucleophilic addition-cyclization process between **1** and **119** afforded the corresponding spirooxindoles **120**. Nucleophilic acyl substitution between **120** and chloroacetyl chloride, followed by S_N2 reaction with isoniazid antibiotic drug, afforded the desired products **121** (Scheme 47). Biologically, the installed C_3-spirooxindoles-isoniazid hybrids (**121**) were evaluated as potential anti-tubercular agents towards *Mycobacterium tuberculosis* H37Rv. Among them, the agent that has two chlorine atoms in benzene and isatin rings (**121a**), was the robust anti-tubercular one with a MIC value of 12.5 μg/mL and an inhibition ability of 81.88 %. Compound **121a** (R = 4-Cl, R_1 = Cl) that showed the robust anti-tubercular activity, also displayed the best binding affinity with the active site of isoniazid-resistant I21V enoyl-ACP(COA) reductase mutant enzyme PDB ID: 2 IE0) via the molecular docking simulation using YASARA software. The best binding mode of **121a** displayed two H-bonds with Gly96 (1.83 and 1.91 Å) through N—H and C═O groups of the side chain. The pyridine N exhibited three H-bonds with Ile16 (4.69 Å), Leu197 (5.35 Å), and Ala198 (3.80 Å). In addition, **121a** was stabilized within the active site through *van der Waals* and a variety of hydrophobic interactions with several amino acids, including Gly14, Ile16, Thr17, Ser19, Ser20, Phe41, Asp42, Arg43, Ser94, Ile95, Gly96, Phe97, Met98, Met103, Ile122, Thr196, Leu197, Ala198, Ile202, and Leu207, proving the potency of **121a**. The authors did not examine the stereochemistry of **121** [60].

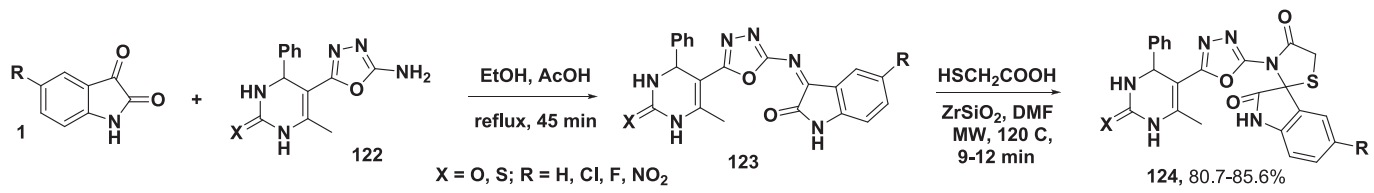

Scheme 48. Chemical construction of C_3-spirooxindoles-linked thiazolidine core **124**.

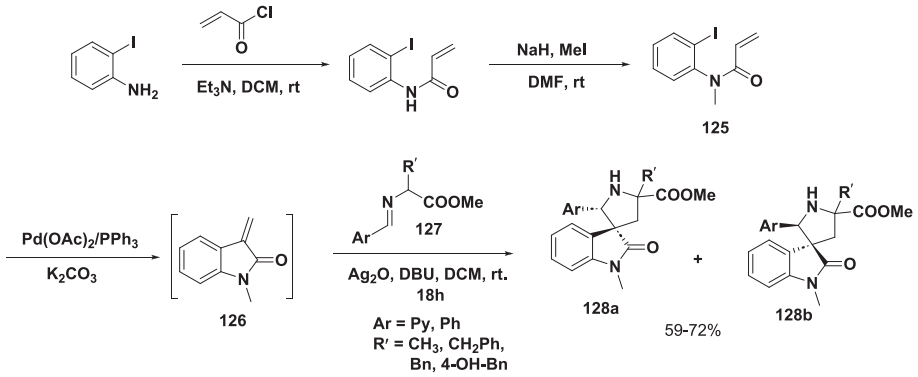

Scheme 49. Chemical construction of C_3-spirooxindoles-linked pyrrolidine moiety **128a,b**.

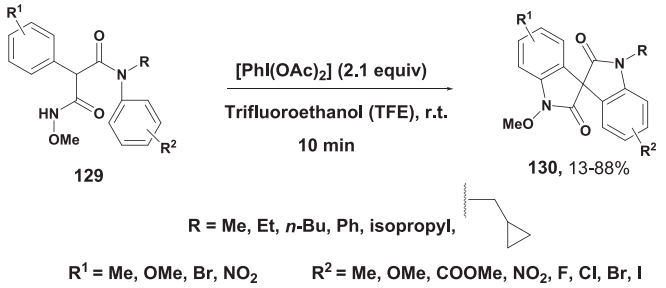

Scheme 50. Chemical construction of C_3-asymmetrical spirooxindoles **130**.

The chemical creation of C_3-spirooxindoles-linked thiazolidine core **124** was published by Borad *et al.* via a domino nucleophilic addition-cyclization reaction of isatin-derived imines **123** (formed from condensation of **1** and **122**) with thioglycolic acid. The process was promoted by MW heating tool in the presence of $ZrSiO_2$ (Scheme 48). Biologically speaking, the installed C_3-spirooxindole-thiazolidine hybrids **124** were tested as potential anti-tubercular agents towards *Mycobacterium tuberculosis*. Among them, agent in which R = NO_2 and X = O (**124a**), was the robust anti-tubercular one with MIC value of 12.5 μg/mL relative to isoniazid (MIC = 0.2 μg/mL). The authors did not examine the stereochemistry of **124**. Compound **124a** was docked against a long-chain enoyl-acyl carrier protein reductase (InhA) (PDB ID: 1ZID) using YASARA software. The best docking mode (11.4740 kcal/mol) showed that the pyrimidine O atom forms an important H-bond with Val65 (3.15 Å) [61].

3. Synthesis of C_3-spirooxindoles via the construction of the oxindole ring using *N*-arylamides as advanced protocols

In 2018, Millington and his research group successfully published the

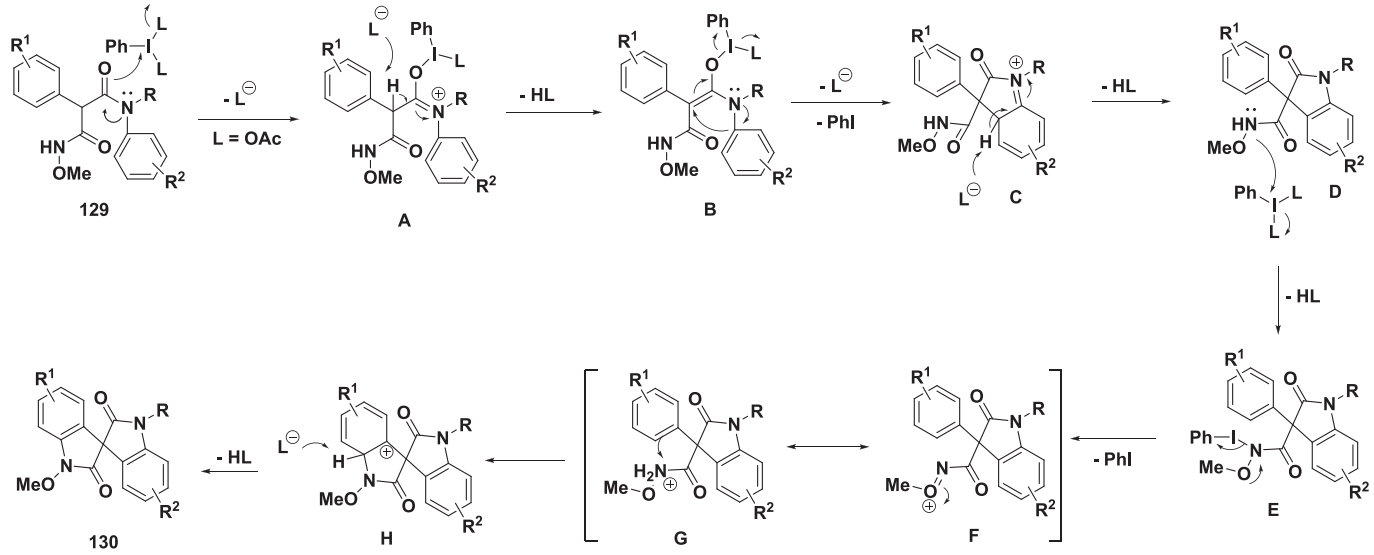

Fig. 16. The proposed mechanism for the construction of **130**.

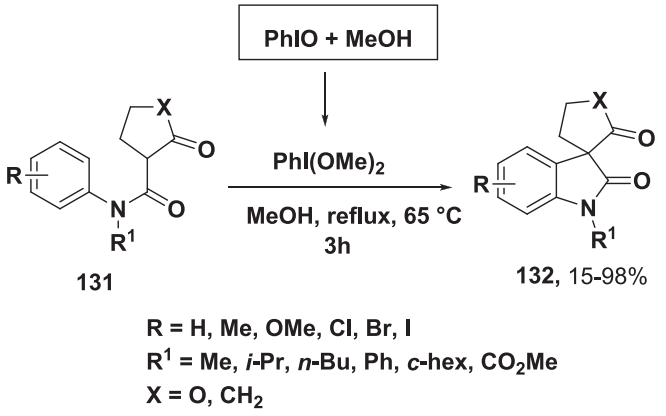

Scheme 51. Chemical construction of C_3-spirooxindoles-containing cyclopentanonyl or lactone moiety **132**.

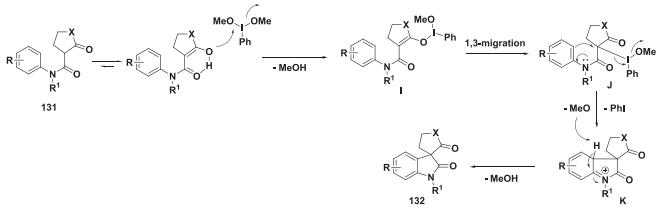

Fig. 17. The proposed mechanism for the construction of **132**.

synthesis of C_3-spirooxindoles-linked pyrrolidine moiety **128a,b** through a combined [Pd(0)/Ag(I)] catalytic system that triggers Heck-1,3-dipolar cycloaddition domino process between *N*-arylamide **125** (that converted to intermediate **126**) and imine derivatives **127** (Scheme 49). The domino process generates azomethine ylides and dipolarophiles *in situ* and gives two new rings with three stereocenters in high yields. The authors did not report the bioactivity of **128a,b** [62].

Also, in 2018, Sun and co-researchers reported a new method to install a library of C_3-asymmetrical spirooxindoles **130** in poor to high yields (13–88 %) using diphenylmalonamides **129** through an intramolecular oxidative domino C—N/C—C bond formation process (Scheme 50). This construction was catalyzed by hypervalent phenyliodine(III) diacetate [PIDA, $PhI(OAc)_2$] as an oxidant at ambient temperature and utilizing TFE as a solvent. Mechanistically, as a nucleophile, the carbonyl oxygen of the *N*-alkyl tertiary amide attacks the iodine atom of the oxidant PIDA to kick out one of the acetate ions, and resulting in an intermediate **A**. Next, the prior intermediate lost the acidic α-proton to form enamine **B**, which went through an intramolecular cyclization process to afford the intermediate imine salt **C**. An oxindole **D** was installed after the aromatization of **C**. After that, the second round of nucleophilic attack on PIDA by the nitrogen atom of the *N*-methoxy secondary amide exhibited intermediate **E** that converted to intermediate **F**/**G** after losing the acetate anion and phenyl iodide. Finally, intramolecular cyclization of **G** and aromatization of **H** yielded the desired C_3-spirooxindoles (**130**) (Fig. 16). The authors did not report the stereochemistry and bioactivity of **130** [63].

After that, in 2019, Zhen and his co-authors reported a modified protocol to prepare C_3-spirooxindoles-containing cyclopentanonyl or lactone moiety **132** using *N*-arylamides **131** through intramolecular oxidative cyclization (Scheme 51). Oxidative $C(sp^2)$—$C(sp^3)$ bond creation was mediated by hypervalent iodine regent phenyliodine (III) dimethoxide [$PhI(OMe)_2$] as an oxidant, which was installed *in situ* by the solvolysis of iodosobenzene (PhIO) with methanol. Fig. 17 shows the proposed mechanism for the formation of **132**. Initially, *N*-arylamide **131** is tautomerized into its enol form, which is stabilized by the intramolecular H-bond. The oxygen atom attacks as a nucleophile on the iodine center of the oxidant phenyliodine(III) dimethoxide to form intermediate **I** that was transformed to the counterpart **J** by 1,3-sigmatropic rearrangement. Intramolecular cyclization of **J** afforded the corresponding imine intermediate **K**, which aromatized to the final product **132**. The authors did not report the stereochemistry and bioactivity of **132** [64].

In 2020, Wang and his colleagues used a dinuclear zinc catalyst to create C_3-spirooxindoles-incorporated chiral tetrahydrofuran **134** via an asymmetric synthesis pathway. Michael-hemiketalization is followed by the Friedel-Crafts process in this case. In the first stage, α-hydroxyacetophenone is treated with β,γ-unsaturated-α-ketoamide **133** in DCM solvent at 20 °C, promoted by a zinc-based catalyst. In the second stage, trifluoroacetic acid was introduced (Scheme 52). The authors did not report the bioactivity of **134** [65].

Luo *et al.* reported a novel method to synthesize the C_3-spirooxindoles-linked phenanthrene moiety **136** via the domino C—H activation process of acrylamides **135** with two moles of iodobenzenes (Scheme 53). As shown in Fig. 18, palladium-catalyzed successive triple C—H activation and four C—C bond creation is based on the double trapping of palladacycle intermediates that are generated by remote C—H activation. The authors did not report the bioactivity of **136** [66].

4. Outlook and conclusion

In the chemical biology community, the development of innovative synthetic techniques and possible therapeutics has acquired considerable momentum and a continuing topic in organic and medicinal chemistry research. C_3-Spirooxindoles are a prominent heterocyclic

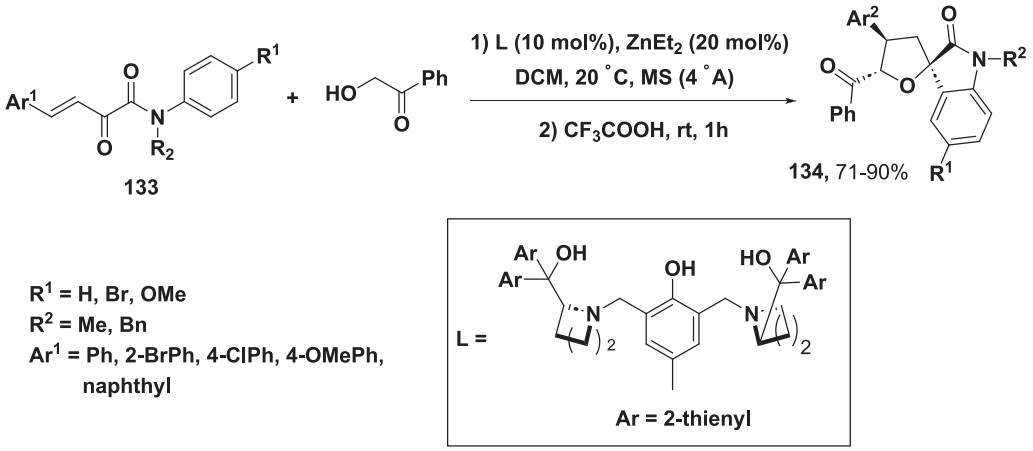

Scheme 52. Chemical construction of C_3-spirooxindoles-linked chiral tetrahydrofuran **134**.

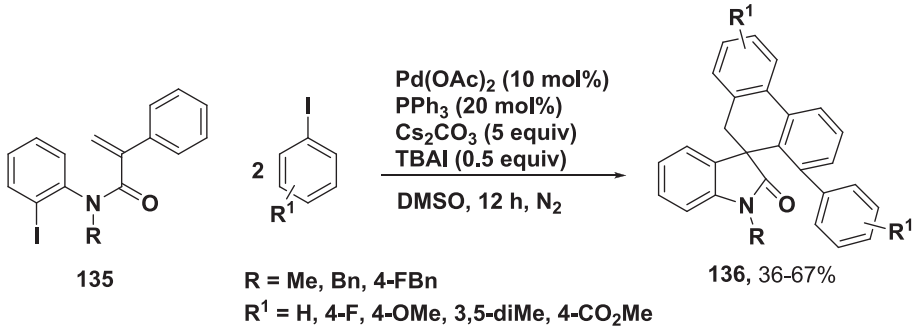

Scheme 53. Chemical construction of C_3-spirooxindoles-linked phenanthrene moiety **136**.

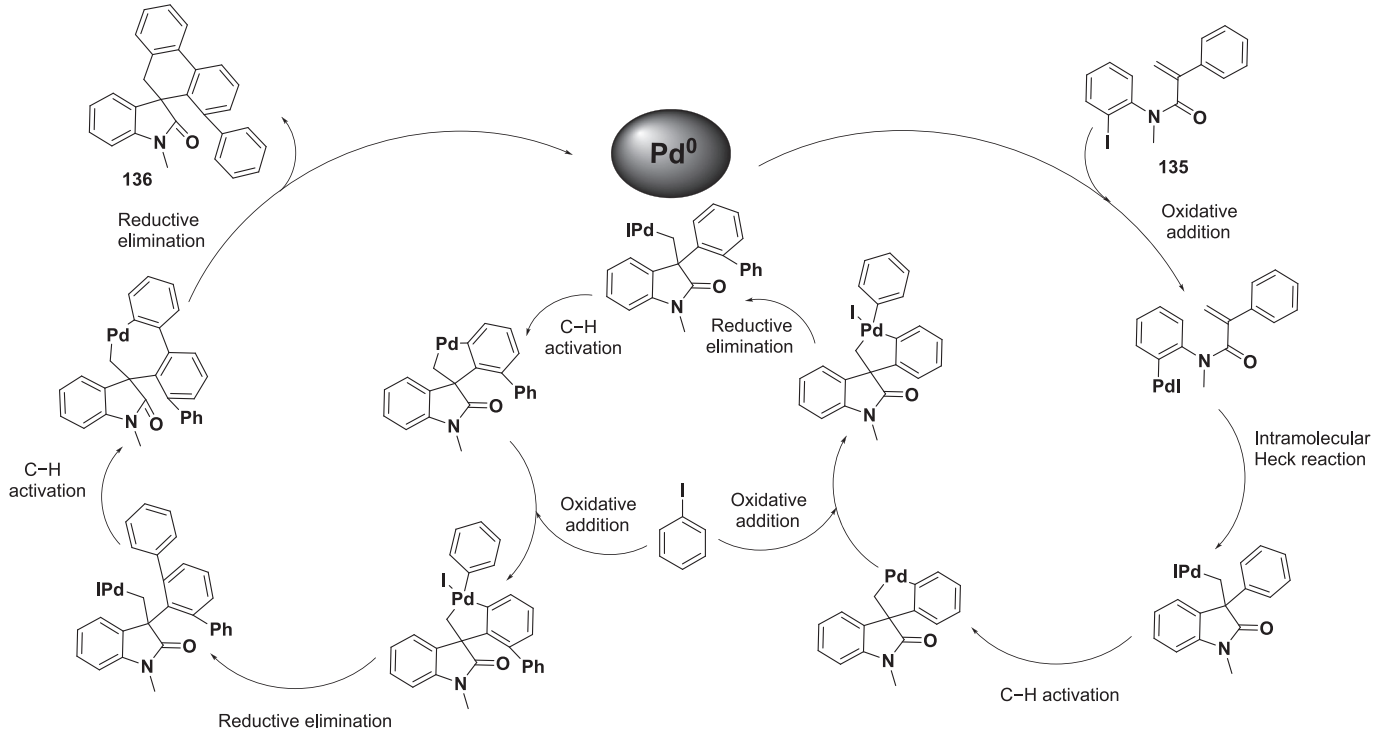

Fig. 18. The proposed mechanism for the construction of **136** (R = Me, R^1 = H).

chemical family that has emerged as intriguing scaffolds with various structural designs and a diverse spectrum of pharmacological properties. Many natural and synthetic compounds have been identified as potential pharmacophores. As previously noted, despite several important breakthroughs and excellent results on C_3-spirooxindoles as potential therapeutic agents, challenges and chances for organic and medicinal chemists remain. Several investigations on C_3-spirooxindole scaffolds have been described and studied in recent years. From our perspectives, we think that the existing synthetic protocols and the enhanced approaches for C_3-spirooxindole scaffolds will provide an effective framework for generating a new generation of potential C_3-spirooxindole analogues that will be employed for a wide range of applications, especially as bioactive lead candidates for drug discovery and development in the future.

CRediT authorship contribution statement

Mohamed H. Helal: Conceptualization. **Medhat E. Owda:** Resources. **Amal T. Mogharbel:** Resources. **Ali Hamzah Alessa:** Resources. **Noha Omer:** Resources. **Mahmoud A. Abdelaziz:** Investigation. **Islam Ibrahim:** Visualization. **Essam M. Eliwa:** Writing – original draft, Writing – review & editing.

Declaration of competing interest

The authors declare that they have no known competing financial interests or personal relationships that could have appeared to influence the work reported in this paper.

Data availability

The data reported in this review article is available on the internet, as stated in the references stated below. The authors also confirm that the data supporting the findings of this study is available within the article.

Acknowledgements

The authors extend their appreciation to the Deanship of Scientific Research at Northern Border University, Arar, KSA for funding this research work through the project number “NBU-FFR-2023-0190”. Also, we are grateful to Al-Azhar University, Faculty of Science, Department of Chemistry, Cairo, Egypt for their continuous support.

References

[1] S.E. John, S. Gulatia, N. Shankaraiah, Recent advances in multi-component reactions and their mechanistic insights: a triennium review, Org. Chem. Front. 8 (2021) 4237–4287, https://doi.org/10.1039/D0QO01480J.

[2] P.V. Saranya, M. Neetha, T. Aneeja, G. Anilkumar, Transition metal-catalyzed synthesis of spirooxindoles, RSC Adv. 11 (2021) 7146–7179, https://doi.org/10.1039/d1ra00139f.

[3] B. Borah, N.S. Veeranagaiah, S. Sharma, M. Patat, M.S. Prasad, R. Pallepogu, L. R. Chowhan, Stereoselective synthesis of CF 3-containing spirocyclic-oxindoles using N-2, 2, 2-trifluoroethylisatin ketimines: an update, RSC Adv. 13 (2023) 7063–7075, https://doi.org/10.1039/d3ra00017f.

[4] A. Deepthi, N.V. Thomas, V. Sathi, Green Protocols for the Synthesis of 3,3'-spirooxindoles – 2016- mid 2019, Curr. Green Chem. 6 (2019) 210–225, https://doi.org/10.2174/2213346106666191019144116.

[5] S.S. Panda, A.S. Girgis, M.N. Aziz, M.S. Bekheit, Spirooxindole: A Versatile Biologically Active Heterocyclic Scaffold, Molecules. 28 (2023) 618, https://doi.org/10.2174/1389557516666160624125108.

[6] J. Bariwal, L.G. Voskressensky, E.V. Van der Eycken, Recent advances in spirocyclization of indole derivatives, Chem. Soc. Rev. 47 (2018) 3831–3848, https://doi.org/10.1039/C7CS00508C.

[7] M. Ganesh, S. Suraj, Expeditious entry into carbocyclic and heterocyclic spirooxindoles, Org. Biomol. Chem. 20 (2022) 5651–5693, https://doi.org/10.1039/D2OB00767C.

[8] L. Wu, Y. Liu, Y. Li, Synthesis of spirooxindole-O-naphthoquinone-tetrazolo [1, 5-a] pyrimidine hybrids as potential anticancer agents, Molecules. 23 (2018) 2330, https://doi.org/10.3390/molecules23092330.

[9] R. Ghosh, J.B. Vitor, E. Mendes, A. Paulo, P.C. Acharya, Stereoselective synthesis of spirooxindole derivatives using one-pot multicomponent cycloaddition reaction and evaluation of their antiproliferative efficacy, ACS Omega. 5 (2020) 27332–27343, https://doi.org/10.1021/acsomega.0c03675.

[10] S. Mayakrishnan, D. Kathirvelan, Y. Arun, K. Saranraj, C. Balachandran, S. Aoki, P. Yuvaraj, N.U. Maheswarai, Design and synthesis of spirooxindole–pyrrolidines embedded with indole and pyridine heterocycles by multicomponent reaction: anticancer and in silico studies, New J. Chem. 46 (2022) 10089–10106, https://doi.org/10.1039/d1nj05839h.

[11] S. Wang, F.-E. Chen, Small-molecule MDM2 inhibitors in clinical trials for cancer therapy, Eur. J. Med. Chem. 236 (2022) 114334, https://doi.org/10.1016/j.ejmech.2022.114334.

[12] N. Koo, A.K. Sharma, S. Narayan, Therapeutics targeting p53-MDM2 interaction to induce cancer cell death, Int. J. Mol. Sci. 23 (2022) 5005, https://doi.org/10.3390/ijms23095005.

[13] M. Kim, J.K. Laramy, G. Gampa, K.E. Parrish, R. Brundage, J.N. Sarkaria, W. F. Elmquist, Brain distributional kinetics of a novel MDM2 inhibitor SAR405838: Implications for use in brain tumor therapy, Drug Metab. Dispos. 47 (2019) 1403–1414, https://doi.org/10.1124/dmd.119.088716.

[14] R.P. Wurz, V.J. Cee, Targeted degradation of MDM2 as a new approach to improve the efficacy of MDM2-p53 inhibitors, J. Med. Chem. 62 (2018) 445–447, https://doi.org/10.1021/acs.jmedchem.8b01945.

[15] A. Gollner, H. Weinstabl, J.E. Fuchs, D. Rudolph, G. Garavel, K.S. Hofbauer, J. Karolyi-Oezguer, G. Gmaschitz, W. Hela, N. Kerres, Targeted Synthesis of Complex Spiro [3H-indole-3, 2′-pyrrolidin]-2 (1H)-ones by Intramolecular Cyclization of Azomethine Ylides: Highly Potent MDM2–p53 Inhibitors, ChemMedChem. 14 (2019) 88–93, https://doi.org/10.1002/cmdc.201800617.

[16] M.S. Islam, A.M. Al-Majid, E.N. Sholkamy, A. Barakat, M. Viale, P. Menichini, A. Speciale, F. Loiacono, M. Azam, V.P. Verma, Optimized spirooxindole-pyrazole hybrids targeting the p53-MDM2 interplay induce apoptosis and synergize with doxorubicin in A549 cells, Sci. Rep. 13 (2023) 7441, https://doi.org/10.1038/s41598-023-31209-3.

[17] M. Espadinha, E.A. Lopes, V. Marques, J.D. Amaral, D.J.V.A. Dos Santos, M. Mori, S. Daniele, R. Piccarducci, E. Zappelli, C. Martini, Discovery of MDM2-p53 and MDM4-p53 protein-protein interactions small molecule dual inhibitors, Eur. J. Med. Chem. 241 (2022) 114637, https://doi.org/10.1016/j.ejmech.2022.114637.

[18] G. Lotfy, Y.M.A. Aziz, M.M. Said, H. El Sayed, H. El Sayed, M.M. Abu-Serie, M. Teleb, A. Dömling, A. Barakat, Molecular hybridization design and synthesis of novel spirooxindole-based MDM2 inhibitors endowed with BCL2 signaling attenuation; a step towards the next generation p53 activators, Bioorg Chem. 117 (2021) 105427, https://doi.org/10.1016/j.bioorg.2021.105427.

[19] M.S. Altowyan, S.M. Soliman, M. Haukka, N.H. Al-Shaalan, A.A. Alkharboush, A. Barakat, Synthesis, characterization, and cytotoxicity of new spirooxindoles engrafted furan structural motif as a potential anticancer agent, ACS Omega. 7 (2022) 35743–35754, https://doi.org/10.1021/acsomega.2c03790.

[20] S.-J. Liu, Q. Zhao, C. Peng, Q. Mao, F. Wu, F.-H. Zhang, Q.-S. Feng, G. He, B. Han, Design, synthesis, and biological evaluation of nitroisoxazole-containing spiro [pyrrolidin-oxindole] derivatives as novel glutathione peroxidase 4/mouse double minute 2 dual inhibitors that inhibit breast adenocarcinoma cell proliferation, Eur. J. Med. Chem. 217 (2021) 113359, https://doi.org/10.1016/j.ejmech.2021.113359.

[21] M. Kukushkin, V. Novotortsev, V. Filatov, Y. Ivanenkov, D. Skvortsov, M. Veselov, R. Shafikov, A. Moiseeva, N. Zyk, A. Majouga, Synthesis and biological evaluation of S-, O-and Se-containing dispirooxindoles, Molecules 26 (2021) 7645, https://doi.org/10.3390/molecules26247645.

[22] B. Wang, F. Peng, W. Huang, J. Zhou, N. Zhang, J. Sheng, P. Haruehanroengra, G. He, B. Han, Rational drug design, synthesis, and biological evaluation of novel chiral tetrahydronaphthalene-fused spirooxindole as MDM2-CDK4 dual inhibitor against glioblastoma, Acta Pharm Sin B. 10 (2020) 1492–1510, https://doi.org/10.1016/j.apsb.2019.12.013.

[23] S.T. Al-Rashood, A.R. Hamed, G.S. Hassan, H.M. Alkahtani, A.A. Almehizia, A. Alharbi, M.M. Al-Sanea, W.M. Eldehna, Antitumor properties of certain spirooxindoles towards hepatocellular carcinoma endowed with antioxidant activity, J. Enzyme Inhib. Med. Chem. 35 (2020) 831–839, https://doi.org/10.1080/14756366.2020.1743281.

[24] W.M. Eldehna, D.H. El-Naggar, A.R. Hamed, H.S. Ibrahim, H.A. Ghabbour, H. A. Abdel-Aziz, One-pot three-component synthesis of novel spirooxindoles with potential cytotoxic activity against triple-negative breast cancer MDA-MB-231 cells, J. Enzyme Inhib. Med. Chem. 33 (2018) 309–318, https://doi.org/10.1080/14756366.2017.1417276.

[25] E.A. Fayed, R.R.E. Eldin, A.B.M. Mehany, A.H. Bayoumi, Y.A. Ammar, Isatin-Schiff's base and chalcone hybrids as chemically apoptotic inducers and EGFR inhibitors; design, synthesis, anti-proliferative activities and in silico evaluation, J Mol Struct. 1234 (2021) 130159, https://doi.org/10.1016/j.molstruc.2021.130159.

[26] R.S. Kumar, A.I. Almansour, N. Arumugam, F. Mohammad, D. Kotresha, J. C. Menéndez, Spirooxindole-pyrrolidine heterocyclic hybrids promotes apoptosis through activation of caspase-3, Bioorg Med Chem. 27 (2019) 2487–2498, https://doi.org/10.1016/j.bmc.2019.03.011.

[27] D. Rajaraman, L.A. Anthony, G. Sundararajan, M. Shanmugam, A. Arunkumar, Synthesis, NMR, anti-oxidant, anti-cancer activity, Molecular docking, DFT Calculations and in silico ADME analysis of 3′-benzoyl-4′-phenyl-5′-(piperazin-1-ylmethyl) spiro [indoline-3, 2′-pyrrolidin]-2-one derivatives, J Mol Struct. 1267 (2022) 133551, https://doi.org/10.1016/j.molstruc.2022.133551.

[28] M.S. Islam, H.M. Ghawas, F.F. El-Senduny, A.M. Al-Majid, Y.A.M.M. Elshaier, F. A. Badria, A. Barakat, Synthesis of new thiazolo-pyrrolidine–(spirooxindole) tethered to 3-acylindole as anticancer agents, Bioorg Chem. 82 (2019) 423–430, https://doi.org/10.1016/j.bioorg.2018.10.036.

[29] K. Murali, H.A. Sparkes, K.J. Rajendra Prasad, Regio- and stereoselective synthesis of dispirooxindole-pyrrolocarbazole hybrids via 1,3-dipolar cycloaddition reactions: Cytotoxic activity and SAR studies, Eur J Med Chem. 143 (2018) 292–305, https://doi.org/10.1016/j.ejmech.2017.11.039.

[30] S. Kasaboina, R. Bollu, P.M. Gomedhika, V. Ramineni, K. Korra, S. Roopika, Basaboina, Uma Devi Holagunda, Lingaiah Nagarapu, Naresh Dumala b, Paramjit Grover b, Raju Bathini c, M. Vijjulatha, Novel benzosuberone conjugates as potential anti-proliferative agents: Design, synthesis and molecular docking studies, (2018). J. Mol. Struct. 1180 (2019) 355-362. Doi: 10.1016/j.molstruc.2018.11.072.

[31] A.M. Al-Majid, M. Ali, M.S. Islam, S. Alshahrani, A.S. Alamary, S. Yousuf, M. I. Choudhary, A. Barakat, Stereoselective synthesis of the di-spirooxindole analogs based oxindole and cyclohexanone moieties as potential anticancer agents, Molecules. 26 (2021) 6305, https://doi.org/10.3390/molecules26206305.

[32] M. Pourshab, S. Asghari, M. Tajbakhsh, A. Khalilpour, Diastereoselective sonochemical synthesis of spirocyclopropaneoxindoles and evaluation of their antioxidant and cytotoxic activities, Chem Biodivers. 16 (2019) e1900087.

[33] M.R. Kumar, A. Manikandan, A. Sivakumar, V.V. Dhayabaran, An eco-friendly catalytic system for multicomponent, one-pot synthesis of novel spiro-chromeno indoline-triones and their anti-prostate cancer potentials evaluated via alkaline phosphatase inhibition mechanism, Bioorg Chem. 81 (2018) 44–54, https://doi.org/10.1016/j.bioorg.2018.07.037.

[34] P. Gobinath, P. Packialakshmi, A. Daoud, S. Alarifi, A. Idhayadhulla, S. Radhakrishnan, Grindstone Chemistry: Design, One-Pot Synthesis, and Promising Anticancer Activity of Spiro [acridine-9, 2′-indoline]-1, 3, 8-trione Derivatives against the MCF-7 Cancer Cell Line, Molecules. 25 (2020) 5862, https://doi.org/10.3390/molecules25245862.

[35] A.M.S. El-Sharief, Y.A. Ammar, A. Belal, M.A.M.S. El-Sharief, Y.A. Mohamed, A.B. M. Mehany, G.A.M.E. Ali, A. Ragab, Design, synthesis, molecular docking and biological activity evaluation of some novel indole derivatives as potent anticancer active agents and apoptosis inducers, Bioorg. Chem. 85 (2019) 399–412, https://doi.org/10.1016/j.bioorg.2019.01.016.

[36] L. Ji, Y. Zhou, Q. Yu, Y. Fang, Y. Jiang, Y. Zhao, C. Yuan, W. Xie, Synthesis and anticancer activity of new spirooxindoles incorporating [1, 2, 4] triazolo [3, 4-b] [1, 3, 4] thiadiazine moiety, J. Mol. Struct. 1227 (2021) 129406, https://doi.org/10.1016/j.molstruc.2020.129406.

[37] Y. Huang, Y.-X. Huang, J. Sun, C.-G. Yan, A [3+ 2] cycloaddition reaction for the synthesis of spiro [indoline-3, 3′-pyrrolidines] and evaluation of cytotoxicity towards cancer cells, New J. Chem. 43 (2019) 8903–8910, https://doi.org/10.1039/C9NJ00994A.

[38] N.G. Fawazy, S.S. Panda, A. Mostafa, B.M. Kariuki, M.S. Bekheit, Y. Moatasim, O. Kutkat, W. Fayad, M.A. El-Manawaty, A.A.F. Soliman, Development of spiro-3-indolin-2-one containing compounds of antiproliferative and anti-SARS-CoV-2 properties, Sci Rep. 12 (2022) 13880, https://doi.org/10.1038/s41598-022-17883-9.

[39] J. Xu, X. Xie, N. Ye, J. Zou, H. Chen, M.A. White, P.-Y. Shi, J. Zhou, Design, synthesis, and biological evaluation of substituted 4, 6-dihydrospiro [[1, 2, 3] triazolo [4, 5-b] pyridine-7, 3′-indoline]-2′, 5 (3 H)-dione analogues as potent NS4B inhibitors for the treatment of dengue virus infection, J Med Chem. 62 (2019) 7941–7960, https://doi.org/10.1021/acs.jmedchem.9b00698.

[40] https://www.who.int/news-room/fact-sheets/detail/malaria.

[41] E.A. Lopes, R. Mestre, D. Fontinha, J. Legac, J.V. Pei, M. Sanches-Vaz, M. Mori, A. M. Lehane, P.J. Rosenthal, M. Prudêncio, Discovery of spirooxadiazoline oxindoles with dual-stage antimalarial activity, Eur. J. Med. Chem. 236 (2022) 114324, https://doi.org/10.1016/j.ejmech.2022.114324.

[42] B. Mathebula, K.R. Butsi, R.L. van Zyl, N.C. Jansen van Vuuren, H.C. Hoppe, J. P. Michael, C.B. de Koning, A.L. Rousseau, Preparation and antiplasmodial activity of 3', 4'-dihydro-1'H-spiro (indoline-3, 2'-quinolin)-2-ones, Chem. Biol. Drug Des. 94 (2019) 1849–1858, https://doi.org/10.1111/cbdd.13598.
[43] A. Nayak, H. Saxena, C. Bathula, T. Kumar, S. Bhattacharjee, S. Sen, A. Gupta, Diversity-oriented synthesis derived indole based spiro and fused small molecules kills artemisinin-resistant Plasmodium falciparum, Malar J. 20 (2021) 1–8, https://doi.org/10.1186/s12936-021-03632-2.
[44] R.S. Kumar, P. Antonisamy, A.I. Almansour, N. Arumugam, G. Periyasami, M. Altaf, H.-R. Kim, K.-B. Kwon, Functionalized spirooxindole-indolizine hybrids: Stereoselective green synthesis and evaluation of anti-inflammatory effect involving TNF-α and nitrite inhibition, Eur. J. Med. Chem. 152 (2018) 417–423, https://doi.org/10.1016/j.ejmech.2018.04.060.
[45] G. Lotfy, Y.M.A. Aziz, M.M. Said, E.S.H. El Ashry, E.S.H. El Tamany, A. Barakat, H. A. Ghabbour, S. Yousuf, Z. Ul-Haq, M.I. Choudhary, Synthesis of oxindole analogues, biological activity, and in silico studies, ChemistrySelect. 4 (2019) 10510–10516, https://doi.org/10.1002/slct.201901228.
[46] M. Ben Hammouda, S. Boudriga, K. Hamden, M. Askri, M. Knorr, C. Strohmann, L. Brieger, A. Krupp, M. Snoussi, K. Aouadi, New spiropyrrolothiazole derivatives bearing an oxazolone moiety as potential antidiabetic agent: Design, synthesis, crystal structure, Hirshfeld surface analysis, ADME and molecular docking studies, J. Mol. Struct. 1254 (2022) 132398, https://doi.org/10.1016/j.molstruc.2022.132398.
[47] A. Toumi, S. Boudriga, K. Hamden, M. Sobeh, M. Cheurfa, M. Askri, M. Knorr, C. Strohmann, L. Brieger, Synthesis, antidiabetic activity and molecular docking study of rhodanine-substitued spirooxindole pyrrolidine derivatives as novel α-amylase inhibitors, Bioorg. Chem. 106 (2021) 104507, https://doi.org/10.1016/j.bioorg.2020.104507.
[48] N. Nivetha, R.M. Martiz, S.M. Patil, R. Ramu, S. Sreenivasa, S. Velmathi, Benzodioxole grafted spirooxindole pyrrolidinyl derivatives: Synthesis, characterization, molecular docking and anti-diabetic activity, RSC Adv. 12 (2022) 24192–24207, https://doi.org/10.1039/D2RA04452H.
[49] C. Teja, S.N. Babu, A. Noor, J.A. Daniel, S.A. Devi, F.R.N. Khan, Cu/TEMPO catalyzed dehydrogenative 1, 3-dipolar cycloaddition in the synthesis of spirooxindoles as potential antidiabetic agents, RSC Adv. 10 (2020) 12262–12271, https://doi.org/10.1039/d0ra01553a.
[50] M. Gul, E. Turk Celikoglu, O. Idil, G. Tas, E. Pelit, Synthesis, antimicrobial activity and molecular docking studies of spiroquinoline-indoline-dione and spiropyrazolo-indoline-dione derivatives, Sci. Rep. 13 (2023) 1676, https://doi.org/10.1038/s41598-023-27777-z.
[51] A. Pandey, A. Pandey, R. Dubey, R. Kant, J. Pandey, Synthesis and computational studies of potent antimicrobial and anticancer indolone scaffolds with spiro cyclopropyl moiety as a novel design element, J. Indian Chem. Soc. 99 (2022) 100539, https://doi.org/10.1016/j.jics.2022.100539.
[52] M.A. Salem, A. Ragab, A.A. Askar, A. El-Khalafawy, A.H. Makhlouf, One-pot synthesis and molecular docking of some new spiropyranindol-2-one derivatives as immunomodulatory agents and in vitro antimicrobial potential with DNA gyrase inhibitor, Eur. J. Med. Chem. 188 (2020) 111977, https://doi.org/10.1016/j.ejmech.2019.111977.
[53] R. Nalini, S.M. Basavarajaiah, G.Y. Nagesh, K.R. Reddy, Design, synthesis and biological evaluation of novel isoniazid hybrids, J. Indian Chem. Soc. 99 (2022) 100273, https://doi.org/10.1016/j.jics.2021.100273.
[54] A. Jarrahpour, Z. Jowkar, Z. Haghighijoo, R. Heiran, J.A. Rad, V. Sinou, F. Rouvier, C. Latour, J.M. Brunel, N. Özdemir, Synthesis, in-vitro biological evaluation, and molecular docking study of novel spiro-β-lactam-isatin hybrids, Med. Chem. Res. 31 (2022) 1026–1034, https://doi.org/10.1007/s00044-022-02898-8.
[55] A.A. Radwan, F.K. Aanazi, M. Al-Agamy, G.M. Mahrous, Design, synthesis and molecular modeling study of substituted indoline-2-ones and spiro [indole-heterocycles] with potential activity against Gram-positive bacteria, Acta Pharmaceut. 72 (2022) 79–95, https://doi.org/10.2478/acph-2022-0004.
[56] M. Pourshab, S. Asghari, M. Mohseni, Synthesis and Antibacterial Evaluation of Novel Spiro [indole-pyrimidine] ones, J. Heterocycl. Chem. 55 (2018) 173–180, https://doi.org/10.1002/jhet.3021.
[57] Y. Huang, W. Min, Q.-W. Wu, J. Sun, D.-H. Shi, C.-G. Yan, Facile one-pot synthesis of spirooxindole-pyrrolidine derivatives and their antimicrobial and acetylcholinesterase inhibitory activities, New J. Chem. 42 (2018) 16211–16216, https://doi.org/10.1039/C8NJ03813A.
[58] M. Bolous, N. Arumugam, A.I. Almansour, R.S. Kumar, K. Maruoka, V.C. Antharam, S. Thangamani, Broad-spectrum antifungal activity of spirooxindolo-pyrrolidine tethered indole/imidazole hybrid heterocycles against fungal pathogens, Bioorg Med. Chem. Lett. 29 (2019) 2059–2063, https://doi.org/10.1016/j.bmcl.2019.07.022.
[59] M. Moghaddam-Manesh, E. Sheikhhosseini, D. Ghazanfari, M. Akhgar, Synthesis of novel 2-oxospiro [indoline-3, 4′-[1, 3] dithiine]-5′-carbonitrile derivatives by new spiro [indoline-3, 4′-[1, 3] dithiine]@ Cu (NO3) 2 supported on Fe3O4@ gly@ CE MNPs as efficient catalyst and evaluation of biological activity, Bioorg Chem. 98 (2020) 103751, https://doi.org/10.1016/j.bioorg.2020.103751.
[60] M.A. Borad, D.J. Jethava, M.N. Bhoi, C.N. Patel, H.A. Pandya, H.D. Patel, Novel isoniazid-spirooxindole derivatives: Design, synthesis, biological evaluation, in silico ADMET prediction and computational studies, J. Mol. Struct. 1222 (2020) 128881, https://doi.org/10.1016/j.molstruc.2020.128881.
[61] M.A. Borad, M.N. Bhoi, S.K. Rathwa, M.S. Vasava, H.D. Patel, C.N. Patel, H. A. Pandya, E.A. Pithawala, J.J. Georrge, Microwave-assisted ZrSiO 2 catalysed synthesis, characterization and computational study of novel spiro [indole-thiazolidines] derivatives as anti-tubercular agents, Interdiscip. Sci. 10 (2018) 411–418, https://doi.org/10.1007/s12539-016-0195-2.
[62] E.L. Millington, H.A. Dondas, C.W.G. Fishwick, C. Kilner, R. Grigg, Catalytic bimetalic [Pd (0)/Ag (I) Heck-1, 3-dipolar cycloaddition cascade reactions accessing spiro-oxindoles. Concomitant in situ generation of azomethine ylides and dipolarophile, Tetrahedron 74 (2018) 3564–3577, https://doi.org/10.1016/j.tet.2018.05.017.
[63] J. Sun, G. Li, G. Zhang, Y. Cong, X. An, D. Zhang-Negrerie, Y. Du, Cascade Formation of C3-Unsymmetric Spirooxindoles via PhI (OAc) 2-Mediated Oxidative C− C/C− N Bond Formation, Adv. Synth. Catal. 360 (2018) 2476–2481, https://doi.org/10.1002/adsc.201800314.
[64] X. Zhen, X. Wan, W. Zhang, Q. Li, D. Zhang-Negrerie, Y. Du, Synthesis of spirooxindoles from N-arylamide derivatives via oxidative C (sp2)–C (sp3) bond formation mediated by PhI (OMe) 2 generated in situ, Org. Lett. 21 (2019) 890–894, https://doi.org/10.1021/acs.orglett.8b03741.
[65] Y.-J. Guo, X. Guo, D.-Z. Kong, H.-J. Lu, L.-T. Liu, Y.-Z. Hua, M.-C. Wang, Catalytic asymmetric synthesis of tetrahydrofuran spirooxindoles via a dinuclear zinc catalyst, J. Org. Chem. 85 (2020) 4195–4206, https://doi.org/10.1021/acs.joc.9b03378.
[66] X. Luo, Y. Xu, G. Xiao, W. Liu, C. Qian, G. Deng, J. Song, Y. Liang, C. Yang, Palladium-Catalyzed Tandem Reaction of Three Aryl Iodides Involving Triple C-H Activation, Org Lett. 20 (2018) 2997–3000, https://doi.org/10.1021/acs.orglett.8b00982.